

NAVAL POSTGRADUATE SCHOOL

Monterey, California



THESIS

**A COMPARISON BETWEEN POWER LINE NOISE LEVEL FIELD
MEASUREMENTS AND MAN-MADE RADIO NOISE PREDICTION
CURVES IN THE HIGH FREQUENCY RADIO BAND**

by

James W. Hodge, Jr.

December, 1995

Thesis Advisor:

Richard W. Adler

Approved for public release; distribution is unlimited.

19960411 111

DTIC QUALITY INSPECTED 1

REPORT DOCUMENTATION PAGEForm Approved
OMB No. 0704-0188

Public reporting burden for this collection of information is estimated to average 1 hour per response, including the time reviewing instructions, searching existing data sources gathering and maintaining the data needed, and completing and reviewing the collection of information. Send comments regarding this burden estimate or any other aspect of this collection of information, including suggestions for reducing this burden to Washington Headquarters Services, Directorate for Information Operations and Reports, 1215 Jefferson Davis Highway, Suite 1204, Arlington, VA 22202-4302, and to the Office of Management and Budget, Paperwork Reduction Project (0704-0188), Washington, DC 20503.

1. AGENCY USE ONLY (Leave Blank)		2. REPORT DATE December 1995	3. REPORT TYPE AND DATES COVERED Master's Thesis	
4. TITLE AND SUBTITLE A COMPARISON BETWEEN POWER LINE NOISE LEVEL FIELD MEASUREMENTS AND MAN-MADE RADIO NOISE PREDICTION CURVES IN THE HIGH FREQUENCY RADIO BAND (U)			5. FUNDING NUMBERS	
6. AUTHOR(S) Hodge, James W., Jr.				
7. PERFORMING ORGANIZATION NAME(S) AND ADDRESS(ES) Naval Postgraduate School Monterey, CA 93943-5000			8. PERFORMING ORGANIZATION REPORT NUMBER	
9. SPONSORING/ MONITORING AGENCY NAME(S) AND ADDRESS(ES)			10. SPONSORING/ MONITORING AGENCY REPORT NUMBER	
11. SUPPLEMENTARY NOTES The views expressed in this thesis are those of the author and do not reflect the official policy or position of the Department of Defense or the United States Government.				
12a. DISTRIBUTION / AVAILABILITY STATEMENT Approved for public release; distribution is unlimited.			12b. DISTRIBUTION CODE	
13. ABSTRACT (Maximum 200 words) Radio frequency noise is often the limiting factor in the ability of a communications receiver to discern a desired signal from man-made interference. The predominate man-made radio noise source in the high frequency radio band is gap type breakdown discharges on electric power distribution lines. The International Radio Consultative Committee (CCIR) has published its Report 258 which predicts the level of man-made radio noise in the business, residential, rural, and quiet rural environmental categories. This thesis compares field measurements of gap type breakdown discharge generated noise, made in the high and very high frequency radio bands, to CCIR Report 258 predictions. It is shown that CCIR noise-level predictions correspond to field measurements in the low end of the high frequency band. At higher frequencies the CCIR curve consistently predicts a lower noise-level than was measured in the field. An explanation for the difference between field measurements and CCIR predictions is presented. A trend noticed in the noise-amplitude versus receiver bandwidth data measurements is investigated and leads to the development of a receiver bandwidth adjustment matrix. Using this matrix the noise-power measurements made in one receiver bandwidth can be scaled to a different bandwidth.				
14. SUBJECT TERMS CCIR noise model, high frequency (HF) radio noise, gap breakdown discharge, microsparking, noise prediction, power line noise			15. NUMBER OF PAGES 96	
			16. PRICE CODE	
17. SECURITY CLASSIFICATION OF REPORT Unclassified	18. SECURITY CLASSIFICATION OF THIS PAGE Unclassified	19. SECURITY CLASSIFICATION OF ABSTRACT Unclassified	20. LIMITATION OF ABSTRACT Unlimited	

Approved for public release; distribution unlimited

**A COMPARISON BETWEEN POWER LINE NOISE LEVEL FIELD
MEASUREMENTS AND MAN-MADE RADIO NOISE PREDICTION
CURVES IN THE HIGH FREQUENCY RADIO BAND**

James W. Hodge, Jr.
Captain, United States Marine Corps
B.S., Texas A&M University, 1989

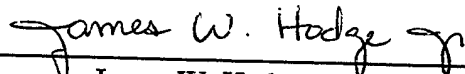
Submitted in partial fulfillment of the
requirements for the degree of

MASTER OF SCIENCE IN ELECTRICAL ENGINEERING

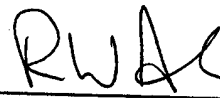
from the

**NAVAL POSTGRADUATE SCHOOL
December 1995**

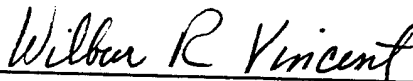
Author:


James W. Hodge, Jr.

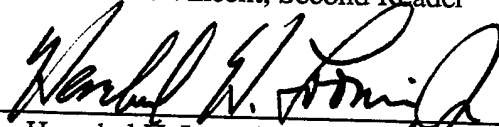
Approved By:



Richard W. Adler, Thesis Advisor



Wilbur R. Vincent, Second Reader



Herschel H. Loomis, Jr., Chairman,
Department of Electrical and Computer Engineering

ABSTRACT

Radio frequency noise is often the limiting factor in the ability of a communications receiver to discern a desired signal from man-made interference. The predominate man-made radio noise source in the high frequency radio band is gap type breakdown discharges on electric power distribution lines. The International Radio Consultative Committee (CCIR) has published its Report 258 which predicts the level of man-made radio noise in the business, residential, rural, and quiet rural environmental categories.

This thesis compares field measurements of gap type breakdown discharge generated noise, made in the high and very high frequency radio bands, to CCIR Report 258 predictions. It is shown that CCIR noise-level predictions correspond to field measurements in the low end of the high frequency band. At higher frequencies the CCIR curve consistently predicts a lower noise-level than was measured in the field. An explanation for the difference between field measurements and CCIR predictions is presented.

A trend noticed in the noise-amplitude versus receiver bandwidth data measurements is investigated and leads to the development of a receiver bandwidth adjustment matrix. Using this matrix the noise-power measurements made in one receiver bandwidth can be scaled to a different bandwidth.

TABLE OF CONTENTS

I. INTRODUCTION	1
A. OVERVIEW	1
B. RADIO NOISE	2
C. BOUNDS	2
D. BACKGROUND	3
II. POWER LINE GENERATED NOISE	5
A. INTRODUCTION	5
B. GAP DISCHARGE MECHANISM(S)	5
1. Spark Type Discharge.....	6
2. Oxide Layer Breakdown Discharge	8
C. ELECTROMAGNETIC COUPLING	10
1. Electromagnetic Noise Radiation.....	11
D. CLASSIC GAP NOISE TEMPORAL STRUCTURE	14
E. SPECTRAL ANALYSIS OF AN IMPULSE	20
III. MAN-MADE NOISE PREDICTION CURVES	31
A. INTRODUCTION	31
B. CCIR REPORT 258: MAN-MADE RADIO NOISE	31
C. CCIR REPORT 322: CHARACTERISTICS AND APPLICATIONS OF ATMOSPHERIC RADIO NOISE DATA	33
D. CCIR REPORT 670: WORLDWIDE MINIMUM EXTERNAL NOISE LEVELS, 0.1 HZ TO 100 GHZ	36

IV. POWER-LINE NOISE FIELD MEASUREMENTS	37
A. INTRODUCTION	37
B. FREQUENCY RANGE: 2 - 8 MHZ	38
C. FREQUENCY RANGE: 10 - 50 MHZ	38
D. FREQUENCY RANGE: 0 - 235 MHZ	38
E. AMPLITUDE VERSUS BANDWIDTH	38
V. ANALYSIS OF FIELD MEASUREMENTS	47
A. INTRODUCTION	47
B. FREQUENCY RANGE 2 TO 8 MHZ	48
C. FREQUENCY RANGE 10 TO 50 MHZ	48
D. FREQUENCY RANGE 0 TO 235 MHZ	48
E. COMMENTS ON THE DIFFERENCES BETWEEN FIELD MEASURED DATA AND CCIR PREDICTED VALUES	52
VI. CONCLUSIONS AND RECOMMENDATIONS	55
A. URBANIZATION, ELECTRIC POWER CONSUMPTION, AND THE LEVEL OF MAN-MADE NOISE	55
B. RECOMMENDATION CONCERNING THE USE OF CCIR REPORT 258	57
C. MITIGATION OF POWER-LINE NOISE	57
APPENDIX A. INSTRUMENTATION	59
A. MEASUREMENT SYSTEM	59
1. Radio Frequency Distribution	59
2. Hewlett-Packard Spectrum Analyzer	60

3. ELF Engineering Model 7200B 3-axis Display	64
4. Tektronix C5-C Camera	65
B. INFORMATION IDENTIFICATION MATRIX	66
APPENDIX B. DATA COLLECTION LOCATIONS	67
A. HAN	67
B. LAH	67
C. MSA DET J	67
D. MSA DET L	68
E. NPS	68
F. WIN	68
LIST OF REFERENCES	71
BIBLIOGRAPHY	75
INITIAL DISTRIBUTION LIST	81

LIST OF SYMBOLS, ACRONYMS AND ABBREVIATIONS

A. SYMBOLS

B	magnetic field vector (T)
E	electric field vector (V/m)
$\nabla \times$	curl of a vector field; del operator and cross product
<i>d</i>	gap distance (cm)
<i>dl</i>	directed differential length-change
<i>ds</i>	differential area: vector with direction normal to the surface
$^{\circ}\text{C}$	degrees Celsius
$^{\circ}\text{F}$	degrees Fahrenheit
ξ	induced electromotive force (V)
λ	lambda (wavelength)
<i>p</i>	pressure (mb)
Φ	magnetic flux crossing surface (Wb)
ρ	air density relative to its value at a pressure 1013 millibar
<i>S</i>	surface
<i>T</i>	temperature in $^{\circ}\text{C}$
<i>t</i>	time (seconds)
<i>V</i>	voltage (volts)
<i>V_s</i>	gap breakdown voltage in kV
Wb	Webers

B. ACRONYMS

CCIR	International Radio Consultative Committee
CDA	Circularly Disposed Antenna Array
FM	frequency modulation
HF	high frequency
HP	Hewlett-Packard
IF	intermediate frequency
LP	log periodic antenna
MSA	mission site activity
NPS	Naval Postgraduate School
RF	radio frequency
RFI	radio frequency interference
SOI	signal of interest
VHF	very high frequency

C. ABBREVIATIONS

avg	average
cm	centimeter
dB	decibel
dBm	decibel (relative to one milliwatt)
Det	detachment
ft	foot
kHz	kilohertz (10^3)
kV	kilovolt
m	meter
min	minute
MHz	megahertz (10^6)
ms	millisecond
ns	nanosecond
sq	square

ACKNOWLEDGMENT

For many years I have carried with me the dream of earning a Master's Degree in Electrical Engineering. Along with that dream was a fervent desire to be under the tutelage of a true Master in his field while I pursued my studies. As though one were not enough, I have been blessed to work with two. These men—my *advisors*—have chosen a most noble pursuit, to skillfully mold others with their knowledge. Professor Adler and Professor Vincent, you hold my deepest respect. It is not possible for a graduate student to have a more capable and competent advisor than either of you. I hope to use well, and build upon, the knowledge you have imparted to me. I sincerely thank you and will always be deeply grateful for what you have allowed me to achieve.

I have also been fortunate to cross the path of some very fine people while I pursued my degree. Truly, without their help I would not have been able to complete this thesis. I gratefully thank George Munsch—another Master in his field—for taking many hours of his time to assist in my education. To Carlos Melnick and Mark and Heesuk Beighey—I very much appreciate your time, patience, and support during my site trips. Not only were you more than helpful, but, your camaraderie allowed me to also enjoy the time I spent abroad. Thank you very much.

Lastly, I would like to dedicate this work to my son, Jim, and my daughter, Jennifer. The love that you have shown me throughout your lives is my inspiration. Without it, I could not have achieved what I have. I love both of you with all my heart. Thank you for being so wonderful.

I. INTRODUCTION

In the solution of telecommunications problems, it is highly desirable to be able to estimate the radio noise at any location as caused by different types of noise sources. At certain locations, unintended man-made noise may be dominant. Since such noise can arise from a number of sources, such as power lines, industrial machinery, ignition systems, etc., it varies markedly with location and time.... [Ref. 1]

A. OVERVIEW

Communication signals that utilize the radiowave portion of the electromagnetic spectrum as their transmission means generally must prevail over diminished field strength (due to range spreading), attenuation, interference, and man-made radio noise, to be successfully received. Within the military there are unique missions, such as direction finding and communications intercept, where the received level of a signal of interest (SOI), even under optimum conditions, is only slightly higher than the equipment noise floor. In such cases, even modest levels of radio-frequency interference (RFI) will mask a SOI. Consequently, to maintain any likelihood of receiving a low-level SOI, it is imperative to not subject the receive system to significant levels of RFI.

This scenario generates the following questions: Where can a receiver site be located to minimize the impact of RFI on the system? What is the RFI level at an existing site? Can RFI be mitigated? The purpose of this thesis is to investigate these questions and propose answers to them.

B. RADIO NOISE

In this thesis *noise* is defined as, "An electromagnetic phenomenon that does not correspond with any signal and that is usually impulsive and random but may be of a periodic nature" [Ref. 2]. Numerous kinds of sources generate radio noise which in turn can become interference to receiving systems. Noise sources are separated into two broad categories: internal to the receiving system and external to the receiving equipment. Internally-generated noise sources are not covered by this effort.

Noise generated externally is further categorized according to its origin: atmospheric, galactic, and man-made. [Ref. 3]

This thesis will investigate man-made radio noise from external sources. Specifically, radio frequency noise generated on electric-power distribution lines by gap-type spark discharges and gap-discharge breakdowns. This noise type, collectively called *gap breakdown noise*, was the predominate man-made RFI source affecting the radio equipment used during this investigation.

C. BOUNDS

The scope of this thesis is primarily concerned with the high frequency (HF) radio band of the electromagnetic spectrum. High frequency signals propagate via ground, direct, and sky waves. Certain properties of the ionosphere allow sky waves to be bent back toward earth. This bending action enables communications over great distances and is an exploited characteristic of HF signals. It is exactly this property that makes the HF radio band important to its users and worthy of investigation. [Ref. 4]

Data was also collected in the very high frequency (VHF) radio band of the electromagnetic spectrum. Very high frequency radio signals do not typically experience the severe amount of bending that HF signals can undergo.

Electromagnetic waves in this band follow a $4/3$ curvature of the earth propagation distance and are more a "line-of-sight" means of communication. Nonetheless, it will be shown that the presence of power line generated noise exists throughout the VHF band and therefore should be considered when determining a potential receiver site location.

Field measurements for this thesis were primarily taken at Wullenweber antenna sites. A Wullenweber antenna, or Circularly Disposed Antenna Array (CDAA), was specifically designed to receive HF signals that have bounced back to earth. Unfortunately, HF noise can also impinge on the antenna array and become RFI. This noise degrades the ability of the CDAA's radio receivers to detect weak signals. The signals that a CDAA site are interested in receiving are generally low in level. Consequently, optimum sites for a CDAA (from an RFI standpoint), are ones that are relatively free of HF radio frequency noise sources. These sites mirror the scenario established in the Overview. Data that were not taken at a CDAA were obtained from log periodic antennas.

D. BACKGROUND

A very large number of investigations of man-made radio noise have been made since the inception of radio communications. Many of these measurements provided information leading to the formulation of a generalized model of such noise, commonly called the CCIR model [Ref 1]. This model is widely employed to provide estimates of man-made radio noise levels at both new and old receiving sites. Since man-made radio noise is often highly variable, time changing, and difficult to categorize, precise comparisons between the model and actual conditions at a receiving site are not expected. The extent of the differences are explored in this thesis.

II. POWER LINE GENERATED NOISE

A. INTRODUCTION

Transportation of electrical power is accomplished via transmission and distribution lines. Transmission lines route electricity from the generation plant to a substation. The line voltage (typically greater than 70 kV) is sufficient to exceed the corona inception voltage of a point source. Under certain conditions the electric-field gradient of a conductor will also exceed the corona breakdown voltage. Radio-frequency noise is generated when this breakdown occurs. RFI originating from transmission line corona was not observed during this investigation and consequently did not contribute to the field measurements of power line noise. It will not be considered in the analysis. [Ref. 5 – 13]

Distribution lines route electricity from substations to the consumers. These lines operate at voltages less than 70 kV, thus do not support corona discharges. Distribution lines, however, are plagued with gap-type electrical discharges. When a gap breakdown occurs RF noise is generated. This type of power-line noise is the focus of this thesis. [Ref. 5 – 13]

B. GAP DISCHARGE MECHANISM(S)

Numerous small gaps, either immersed in air or electrically separated by a layer of insulating oxide or corrosion, form between a variety of power line hardware. The gaps are generally associated with loose fitting nuts, bolts, tie wires, guy lines, brackets, ground wires, oxidized insulator clevis joint pins, crossarm braces, and damaged lightning arrestors. Incidental contact between parts can also occur. This is generally due to the wind and can produce intermittent interference (which hampers locating such sources).

1. Spark Type Discharge

When insulated or air gaps are subjected to an electric field (generated by the power line conductors) a difference of potential will develop between the two contacts. For atmospheric air the gap breakdown voltage is given by

$$V_s = 24.4(\rho d) + 6.53\sqrt{(\rho d)} \quad (2.1)$$

where V_s is the breakdown voltage in kV, d is the gap length in cm, and

$$\rho = \frac{p}{1013} \cdot \frac{293}{T + 273} \quad (2.2)$$

is the air density relative to its value at a pressure $p = 1013$ mb and a temperature T in $^{\circ}\text{C}$ [Ref. 5]. Table 2.1 lists gap breakdown voltages for various gap distances in atmospheric air.

Table 2.1: Air Gap Breakdown Voltage.

gap distance (cm)	kV @ 68 $^{\circ}\text{F}$	kV @ 85 $^{\circ}\text{F}$
0.010	0.89	0.88
0.020	1.41	1.38
0.030	1.86	1.82
0.050	2.68	2.62
0.075	3.62	3.53
1.000	30.93	30.07
2.000	58.03	56.37

Note that under normal conditions distribution lines have ample voltage to support gap discharge for a wide range of gap distances.

When the electric field across a gap is strong enough to exceed the breakdown potential of air or other insulation, an ionization process occurs that transforms air from a poor conductor to a good conductor. This process is

based upon free electrons contained within the air gap that are accelerated due to the difference of potential that exists between the gap contacts. The accelerated electrons collide with molecules of gas which ionize and release additional free electrons. These electrons continue the process, multiplying the free electron production rate. If the potential gradient is sufficient, the ionization process will continue until an avalanche chain reaction is initiated which rapidly decreases the gap resistance. At this juncture a channel is formed and a current surge occurs. It is this surge of current that generates radio-frequency noise. [Ref. 6, 11]

If sufficient power is available a continuous flow of current, called an arc, will form across the gap. However, if the gap resistance is too high a stable arc will not form while current surges across the gap. The current surge associated with either of these descriptions is called a spark. [Ref. 6]

As current flows through the formed channel the potential difference across the gap is reduced and the spark is extinguished. Although the spark has been extinguished, it is possible for reignition to occur if the difference of potential across the gap recovers to above the breakdown voltage. Figure 2.1 shows hypothetical sections of a 60-Hz sinusoid that would support an arbitrary gap's voltage breakdown requirement. [Ref. 5, 6, 11, 13]

During each voltage half-cycle of the power-line fundamental frequency, it is typical for the gap potential gradient to exceed the gap breakdown voltage numerous times. Each breakdown generates a current pulse. It is also common for the opposite polarity half-cycles to produce dissimilar noise waveforms. Furthermore, as this process manifests itself through the power-line period, the fundamental frequency (and its harmonics) are superimposed, or modulated, onto the generated radio-frequency noise. Examples of this phenomenon are presented in Section D of this chapter. [Ref. 7, 11, 12]

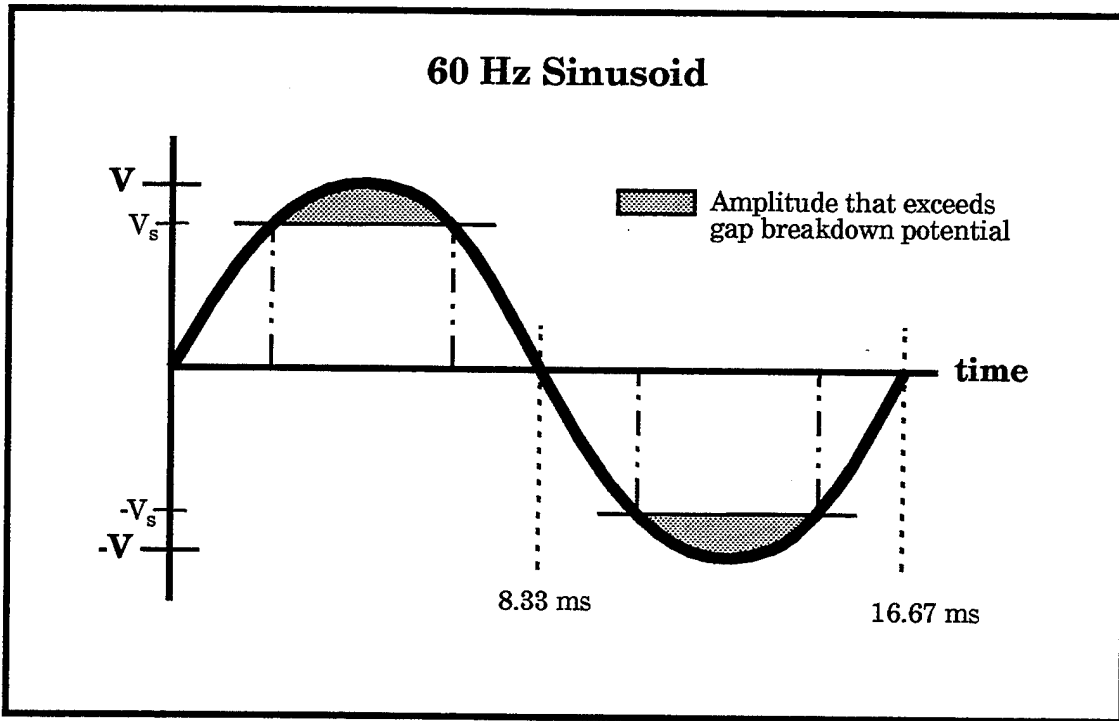


Figure 2.1: Portions of 60-Hz Sinusoid that Support the Potential Difference Required to Exceed a Gap's Breakdown Voltage (and possible spark reignition).

2. Oxide Layer Breakdown Discharge

Some gap discharges evolve because a thin oxide layer has developed between metal parts of an insulator, particularly a bell-type insulator. Figure 2.2 demonstrates how bell-insulators are utilized on power lines. A difference of potential occurs because one side of the insulator is connected to the power line while the other side is connected to the utility pole. Figure 2.3 shows the parts of a bell-insulator that support gap breakdowns. The oxide layer forms between the clevis pin and metal parts of the insulator. The difference of potential required to induce a gap breakdown between the oxide insulated parts can be as low as 800 volts. [Ref. 13]

When an electric field induces a sufficient potential difference across the oxide layer an impulse of current is generated. The current surge reduces

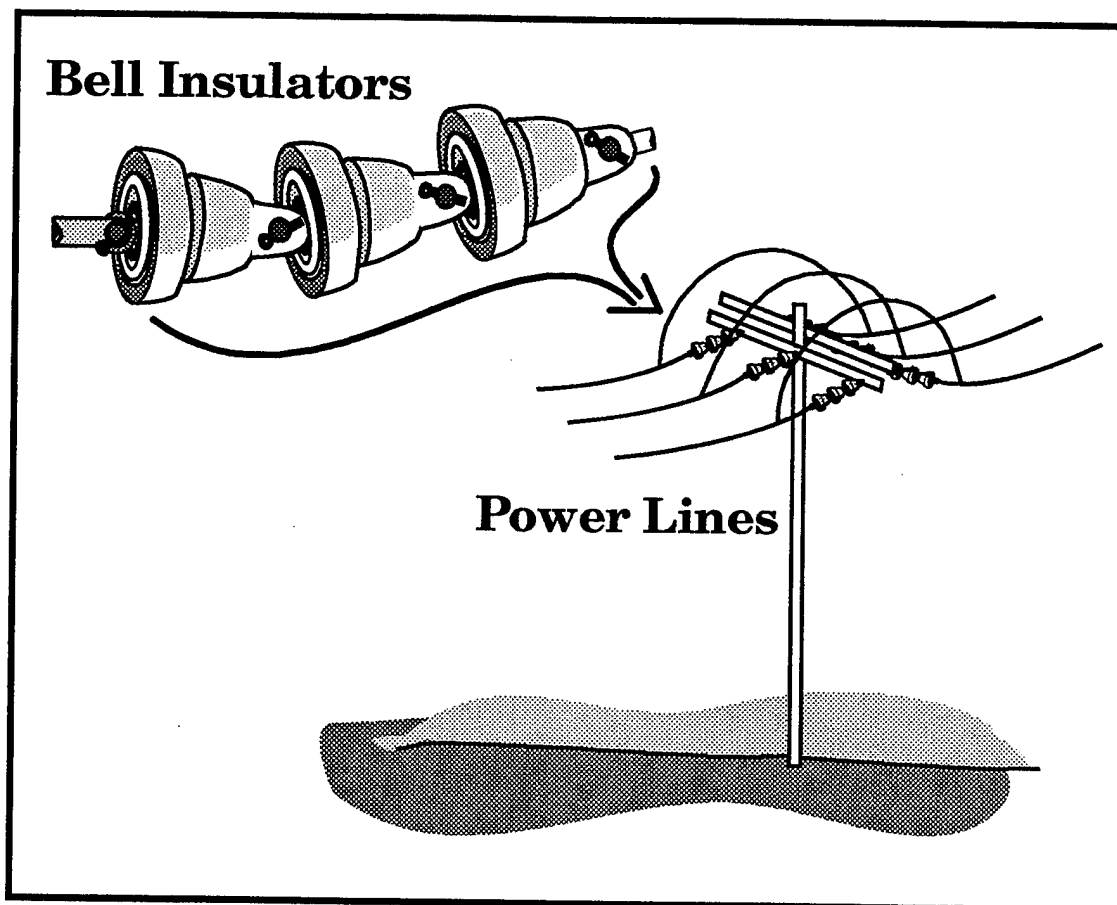


Figure 2.2: Bell Insulators Used on Power Lines.

the difference of potential across the components and the impulse ceases. As with spark type discharges, the electric field magnitude is usually sufficient to generate numerous current surges per power line half-cycle. The oxide layer breakdown discharge is also referred to as microsparking. [Ref. 7, 15, 16]

Oxide layer breakdown is sensitive to meteorological conditions. For instance, if the power line has morning dew, or if there is fog, or if it is raining, the oxide layer on the insulator will be subjected to moisture dissolved impurities that provide a conduction path which precludes the build up of electrons to support a gap discharge. [Ref. 11, 12, 13, 17]

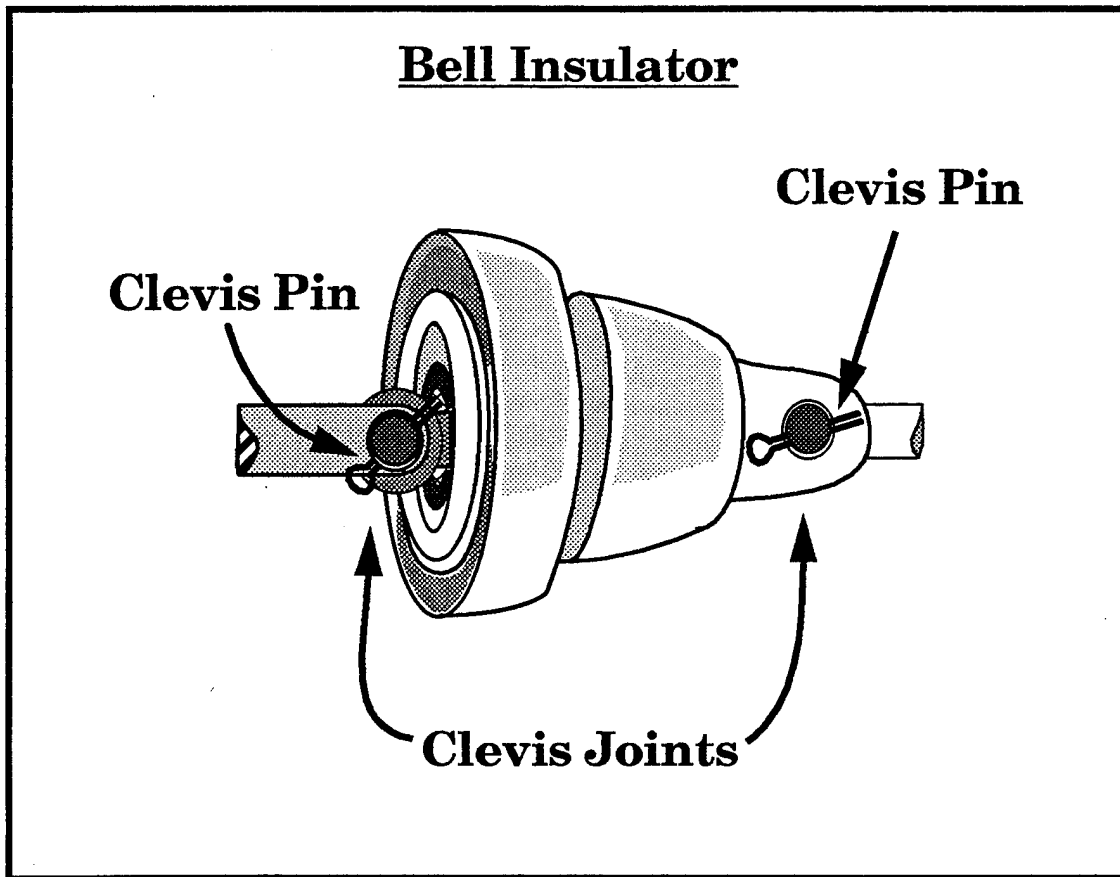


Figure 2.3: Close Up of Bell Insulator Parts.

C. ELECTROMAGNETIC COUPLING

From Faraday's law of induction and Maxwell's second equation we know that a time-varying magnetic field (**B**) generates an electric field (**E**).

$$\nabla \times \mathbf{E} = - \frac{\partial \mathbf{B}}{\partial t} \quad (2.3)$$

That is, taking the surface integral of both sides of Eq. (2.3) over an open surface and applying Stokes's theorem, we obtain

$$\oint_C \mathbf{E} \cdot d\mathbf{l} = - \int_S \frac{\partial \mathbf{B}}{\partial t} \cdot d\mathbf{s} \quad (2.4)$$

If we define

$$\xi = \oint_C \mathbf{E} \cdot d\mathbf{l} = \text{emf induced in circuit with contour } C \text{ (V)} \quad (2.5)$$

and

$$\Phi = \int_S \mathbf{B} \cdot d\mathbf{s} = \text{magnetic flux crossing surface } S \text{ (Wb)}, \quad (2.6)$$

then Eq. (2.4) becomes

$$\xi = -\frac{d\Phi}{dt} \quad (\text{V}) \quad (2.7)$$

The current surge associated with a gap breakdown discharge provides the time-varying magnetic field. The resulting electric field impinges on the power line (or neutral) conductor and establishes a difference of potential on the line which induces current flow at a rate proportional to the charge-discharge cycle of the gap breakdown. As the gap polarity changes, the induced current flow in the power-line conductor modulates the radiated noise with the fundamental frequency (and harmonics generated by non-linearities of the breakdown process) of the power line. This modulation characteristic provides a signature for power-line noise identification. Figure 2.4 outlines the gap breakdown process, referred to as classic gap noise. [Ref. 11, 13]

1. Electromagnetic Noise Radiation

Radiation of the generated noise is accomplished via the power-line conductor (or neutral) which acts as an antenna. The distance between utility poles is conducive to establishing nodes that can set up high-amplitude standing waves on the distribution lines. These standing waves radiate noise energy in the HF and VHF radio bands. [Ref. 16,17]

The radio noise generated by a gap breakdown discharge is a function of numerous independent variables. Some of the variables are gap geometry, oxide layer thickness, meteorological conditions, power-line conductor

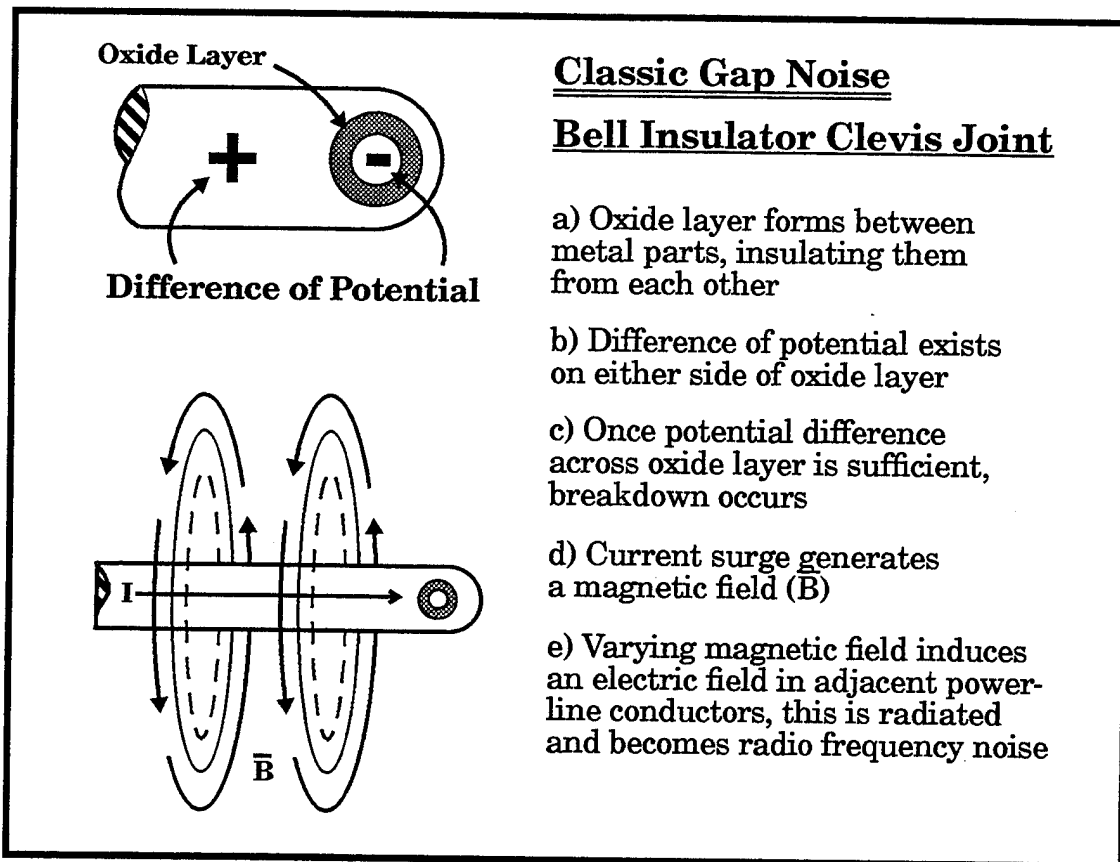
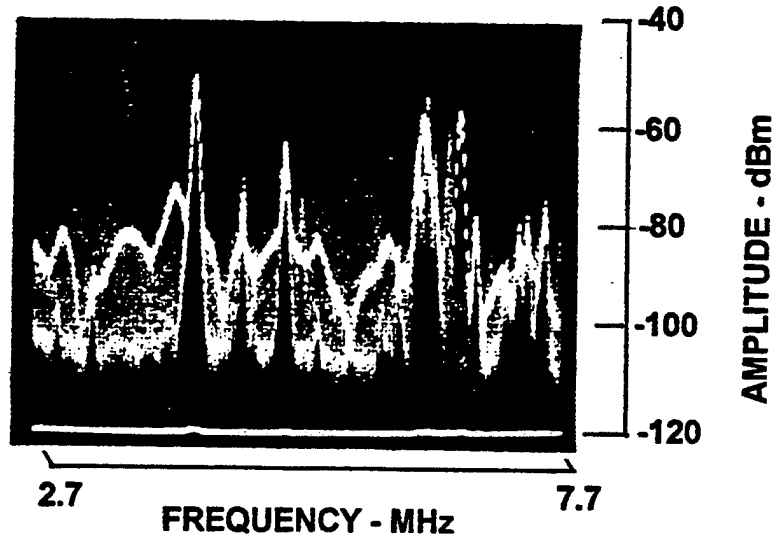
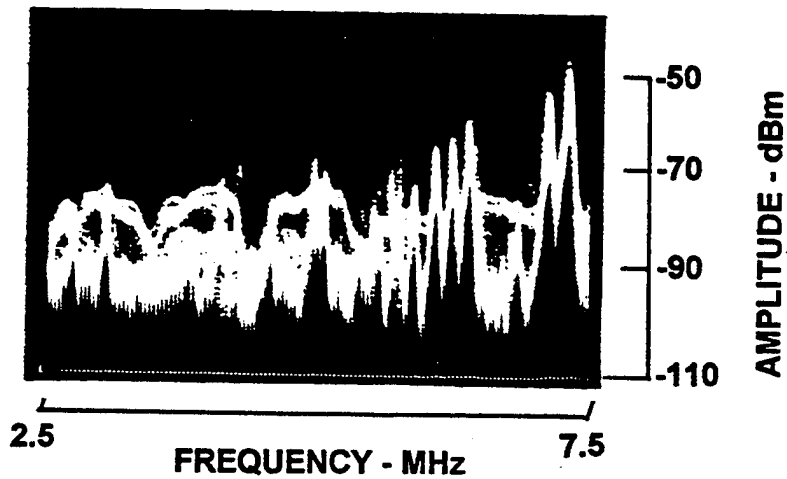


Figure 2.4: Insulator Oxide Layer Gap Breakdown.

pole-to-pole length, distance of the noise source to the receiving antenna, geometry of the noise source relative to all associated hardware, direction of power lines relative to the receive antenna location, the near and far electromagnetic field effects on the radiation pattern due to the associated hardware, the source impedance, and the power line impedance. This is by no means an exhaustive list. The purpose of the list, however, is to caution the reader against characterizing the effects of a gap-type noise source in a specific way and then attempting to apply that characterization to all other antennas that have a gap-type noise source impinging on it. It will be the totality of the afore mentioned factors that will ultimately determine the amplitude and spectral distribution of any local source to the affected antenna. Figure 2.5



950620 1345
 WIN, RFSS, LB 048
 5.2 MHz, 5 MHz, 30 kHz, 200 ms
 BPF 9, +20, 0, -20



950817 1045
 HAN, RFD, LB 000
 5 MHz, 5 MHz, 30 kHz, 1 s
 BPF 9, +20, 0, -10

Figure 2.5: Amplitude and Spectral Distribution of Two Independent Gap-type Noise Sources.

demonstrates the difference in amplitude and spectral distribution between two independent gap-type noise sources. The fundamental lessons learned—albeit an intuitive understanding—concerning the potential effects of gap-type noise sources to a receiving system are achieved through applying Faraday's law of induction, fundamental electromagnetism and antenna theory, and the material that is presented in Section E of this chapter.

D. CLASSIC GAP NOISE TEMPORAL STRUCTURE

The process that a classic gap noise source goes through to generate noise is fundamental to each source. The results of each independent process, however, vary considerably from source to source. The impulsive nature of a gap breakdown discharge produces a distinctive temporal structure for each classic gap noise source. The stability, duration, amplitude, pulse timing, pulse width, and power line half-cycle symmetry are all unique to the individual source.

Appendix A describes the instrumentation, data-collection method, and the information identification scheme that were utilized to collect and identify the following data. Appendix B describes the data-collection locations.

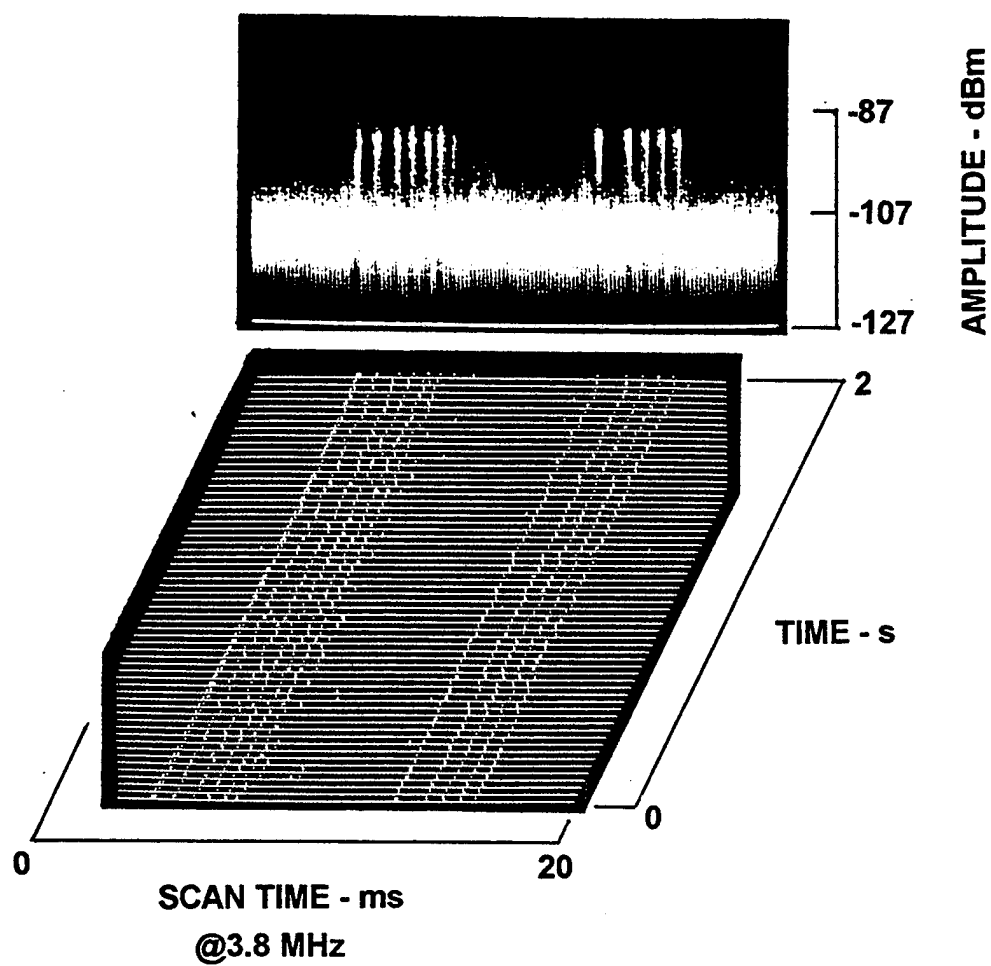
Figure 2.6 displays a classic gap noise source that is regular and stable. It has dissimilar half-cycle gap discharge impulses.

Figure 2.7 shows a persistent classic noise source. The two half-cycles generate different fine-scale structure with the trailing impulses becoming more erratic in time.

Figure 2.8 is a constant classic gap noise source that has dissimilar half-cycle impulses. Note the difference in both amplitude and structure of the impulses even though they are from the same source.

Figure 2.9 shows a sporadic noise source.

Figure 2.10 is an example of how abruptly a classic gap source can start or stop. The trailing impulses of one half-cycle are erratic.



950623 1305
 WIN, RFSS, LB 036
 3.8 MHz, 0, 30 kHz, 20 ms LS
 -3, BPF 9, +20, 0, -30

Figure 2.6: Classic Gap Noise Source. Structure: Regular and Steady.

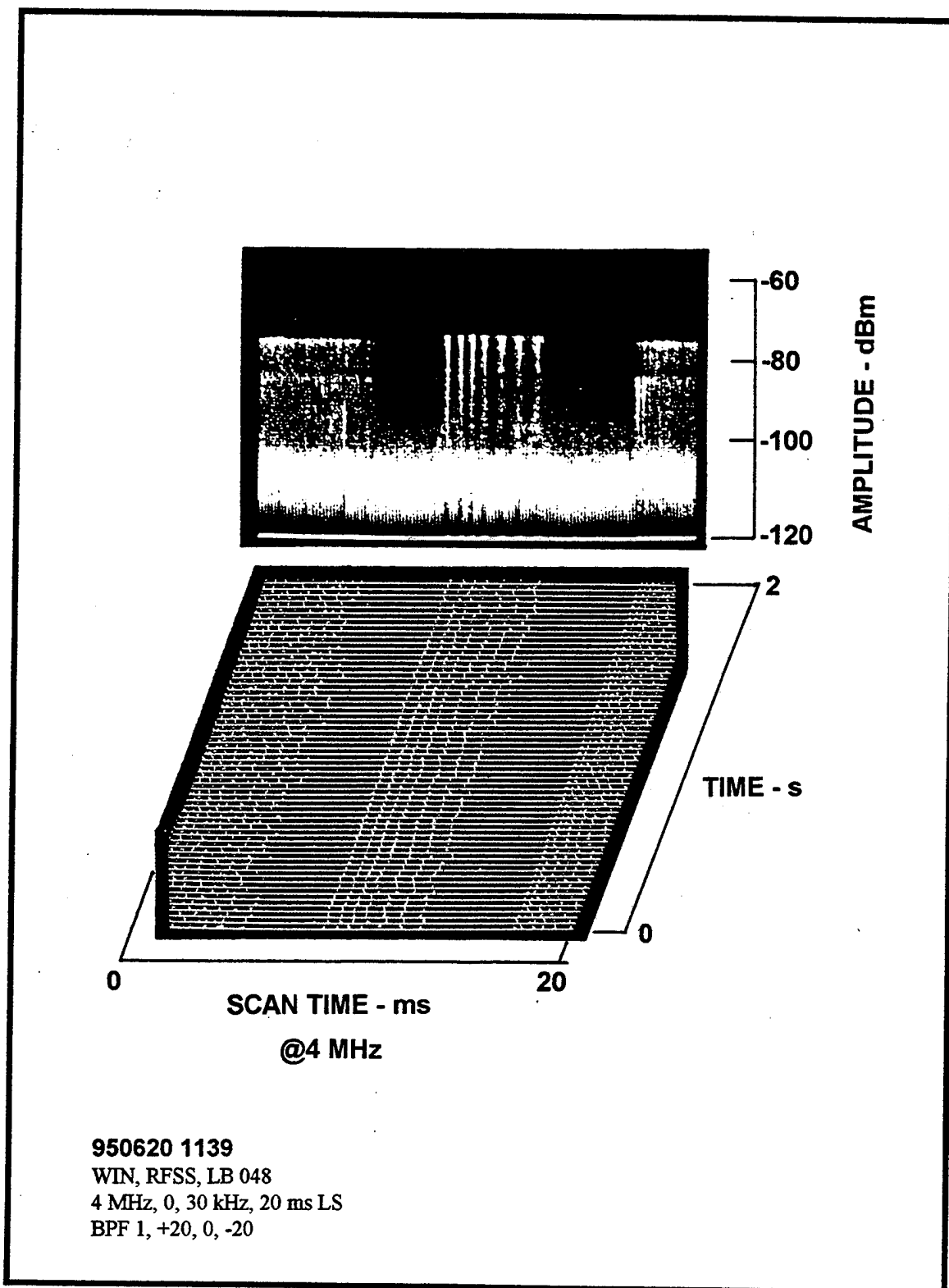
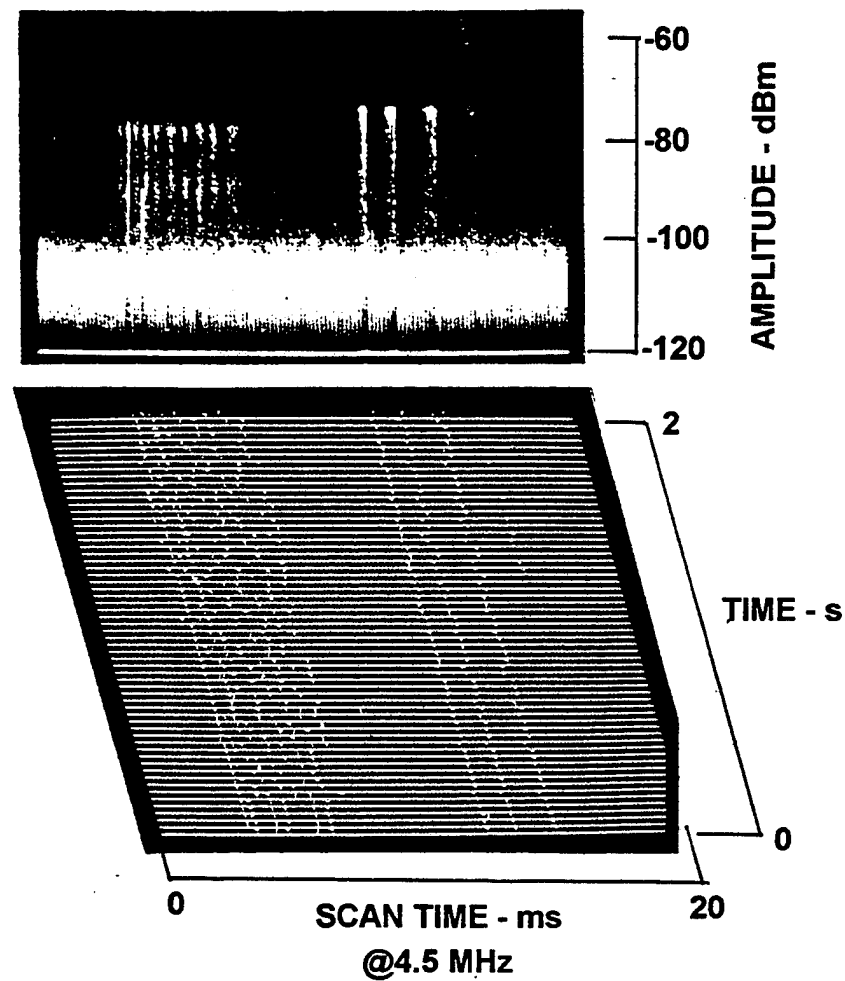
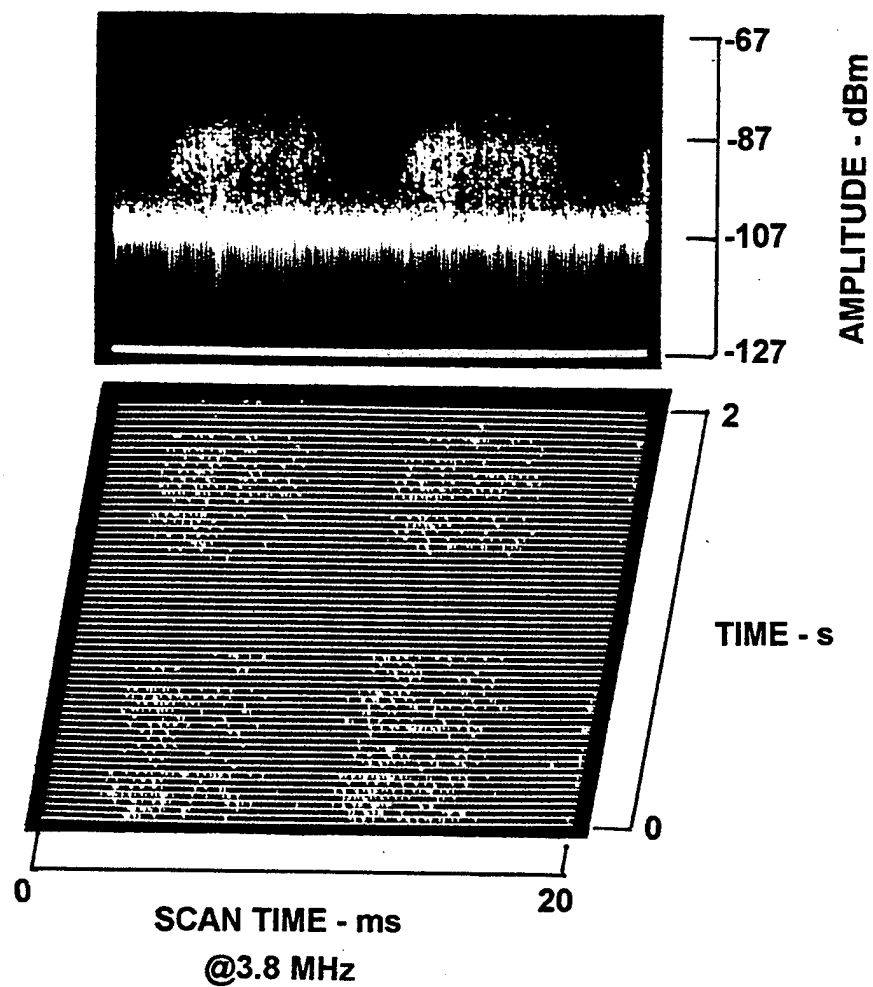


Figure 2.7: Classic Gap Noise Source. Structure: Regular but Different Half-cycle Impulses and Erratic Half-cycle Ending Pulses.



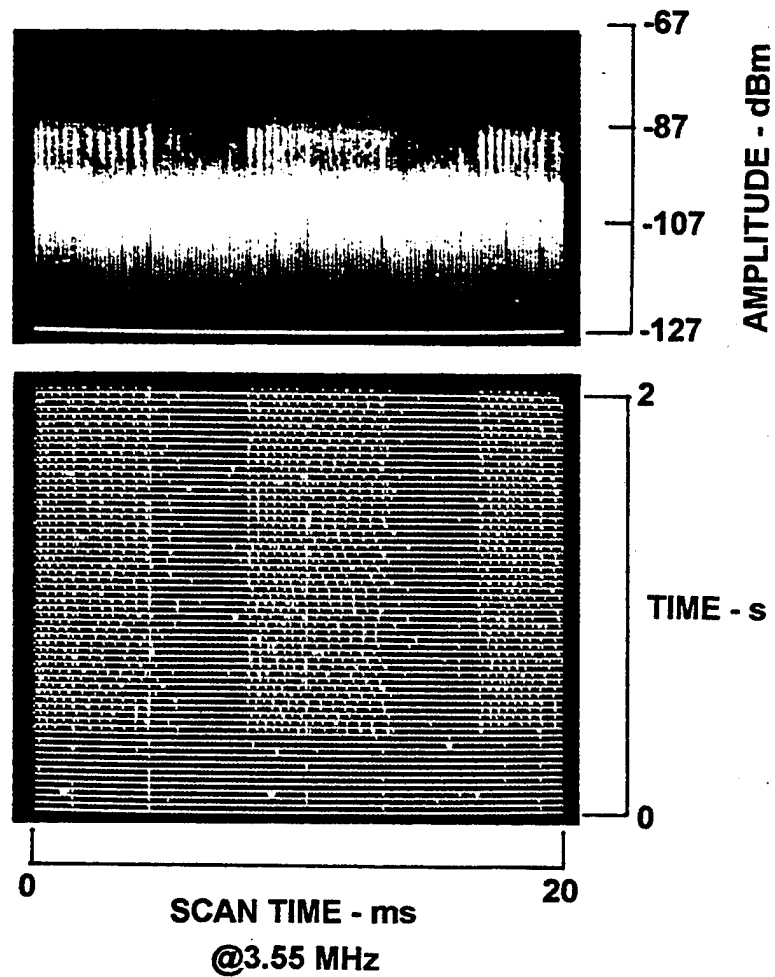
950620 1042
 WIN, RFSS, LB 072
 4.5 MHz, 0, 30 kHz, 200 ms
 BPF 9, +20, 0, -20

Figure 2.8: Classic Gap Noise Source. Structure: Regular but Different Half-cycle Impulses with Intermittent End Pulse on Right Side.



950623 1515
 WIN, RFSS, LB 108
 3.8 MHz, 0, 30 kHz, 20 ms LS
 -3, BPF 9, +20, 0, -30

Figure 2.9: Classic Gap Noise Source. Structure: Sporadic.



950623 1055
 WIN, RFSS, LB 300
 3.55 MHz, 0, 30 kHz, 20 ms LS
 -3, BPF 9, +20, 0, -30

Figure 2.10: Classic Gap Noise Source. Structure: Regular (until abrupt stop) with Erratic Impulse Timing in One Half-cycle.

Figure 2.11 displays a strong classic gap noise source. One half-cycle is constant and the other is unstable.

Figure 2.12 shows a noise source that has dissimilar half-cycle impulse generation. The impulses become erratic near the end of the half-cycle. One half-cycle is intermittent.

Figure 2.13 shows a constant noise source that has unstable impulses.

Figure 2.14 shows two classic gap noise sources. One source is constant with erratic impulses. The other source is intermittent and is active on one half-cycle only.

Figure 2.15 shows multiple sources. One is constant with erratic trailing impulses, one is intermittent, and the other is close to the noise floor and did not show up on the amplitude compressed and threshold limited time-history view.

E. SPECTRAL ANALYSIS OF AN IMPULSE

The previous section demonstrated that the temporal structure of individual classic gap noise sources do not possess uniform parameters. The dissimilarity among individual sources hinders direct analysis of the impulsive nature of a gap-breakdown discharge. Fortunately, we can make an assumption that allows us to ignore the diverse and complex waveforms that the various sources generate. The approach will significantly reduce the difficulty of the analysis, yet, will not diminish our understanding of the effect of a gap-breakdown discharge.

Our assumption is to represent a classic gap discharge impulse as a single ideal square pulse $x(t)$,

$$x(t) = \begin{cases} A_p & , \quad |t| \leq \frac{T}{2} \\ 0 & , \quad \text{otherwise} \end{cases} \quad (2.8)$$

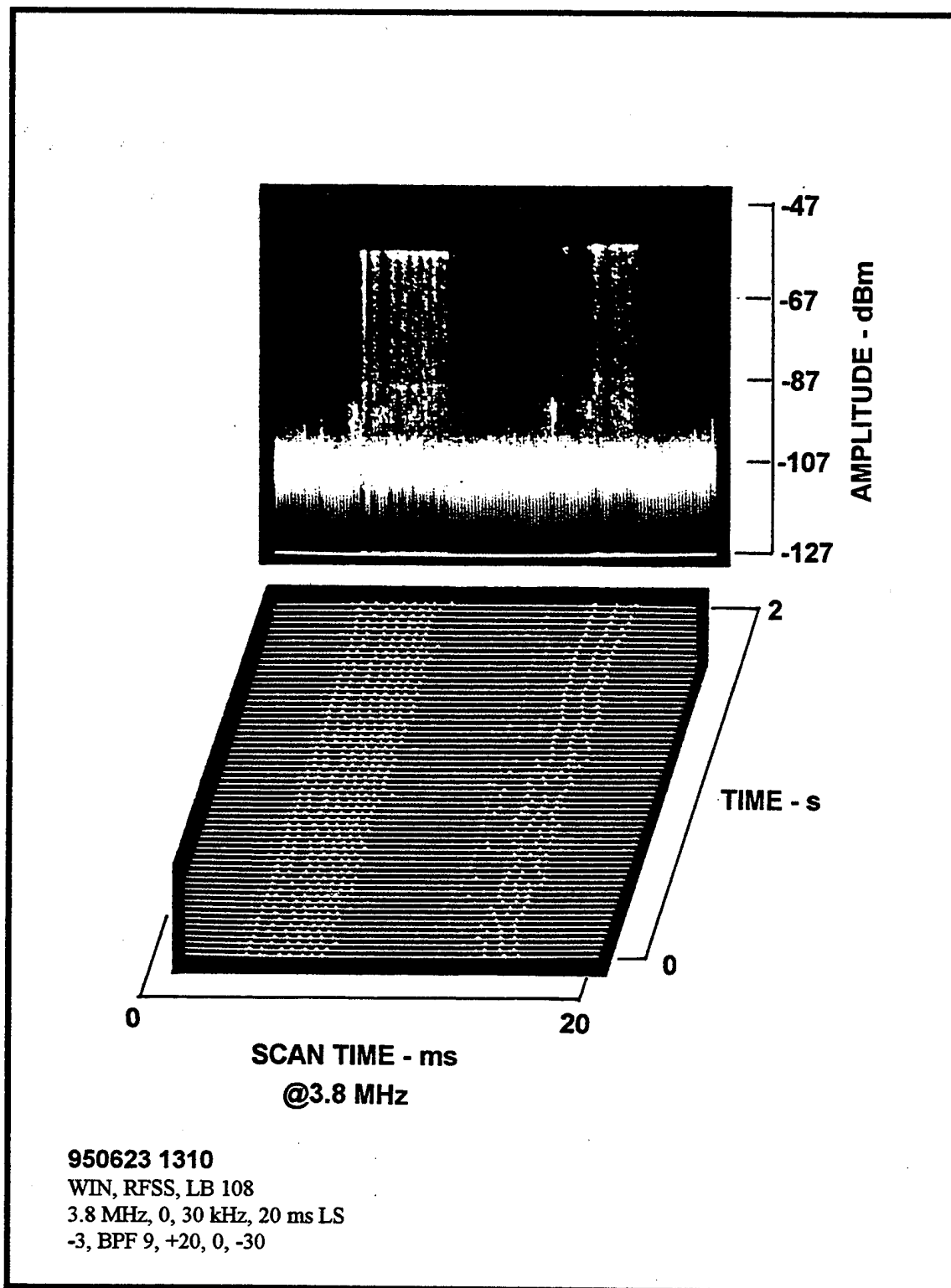
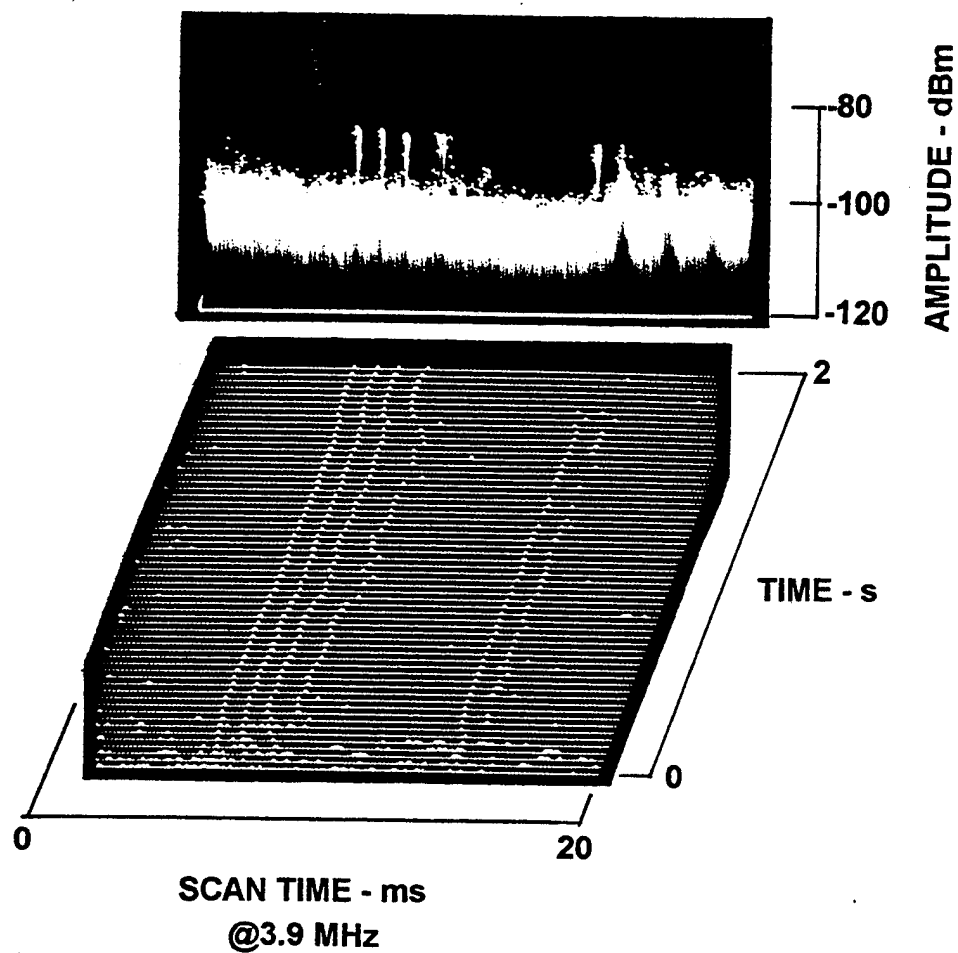
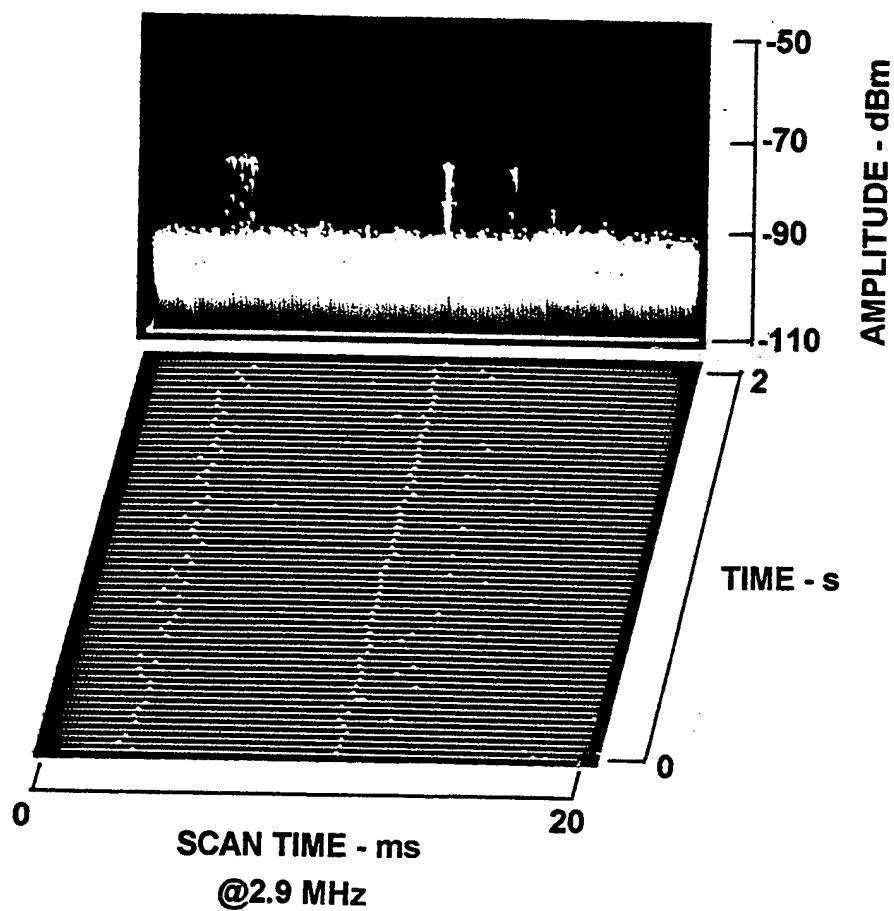


Figure 2.11: Classic Gap Noise Source. Structure: Strong Source, Regular with One Half-cycle Erratic.



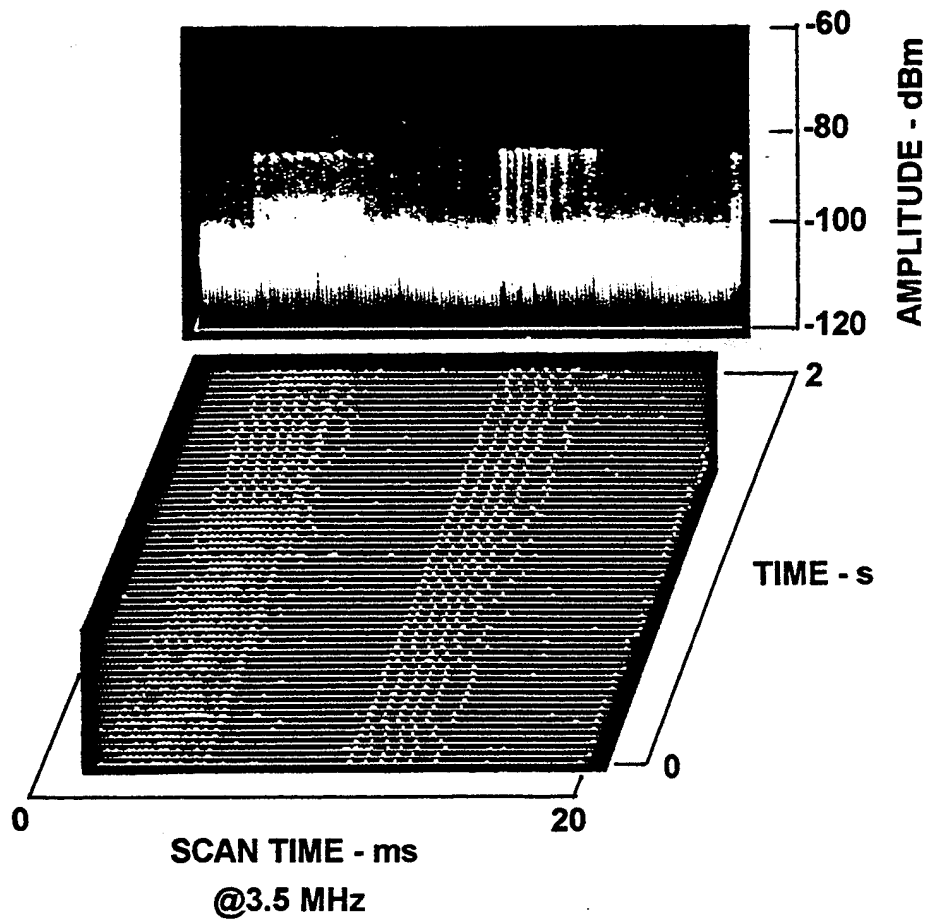
950816 1420
 HAN, RFD, LB180
 3.9 MHz, 0, 30 kHz, 20 ms LS
 BPF 9, +20, 0, -20

Figure 2.12: Classic Gap Noise Source. Structure: Regular for Half-cycle but Intermittent for Other Half-cycle, Impulse Timing Erratic.



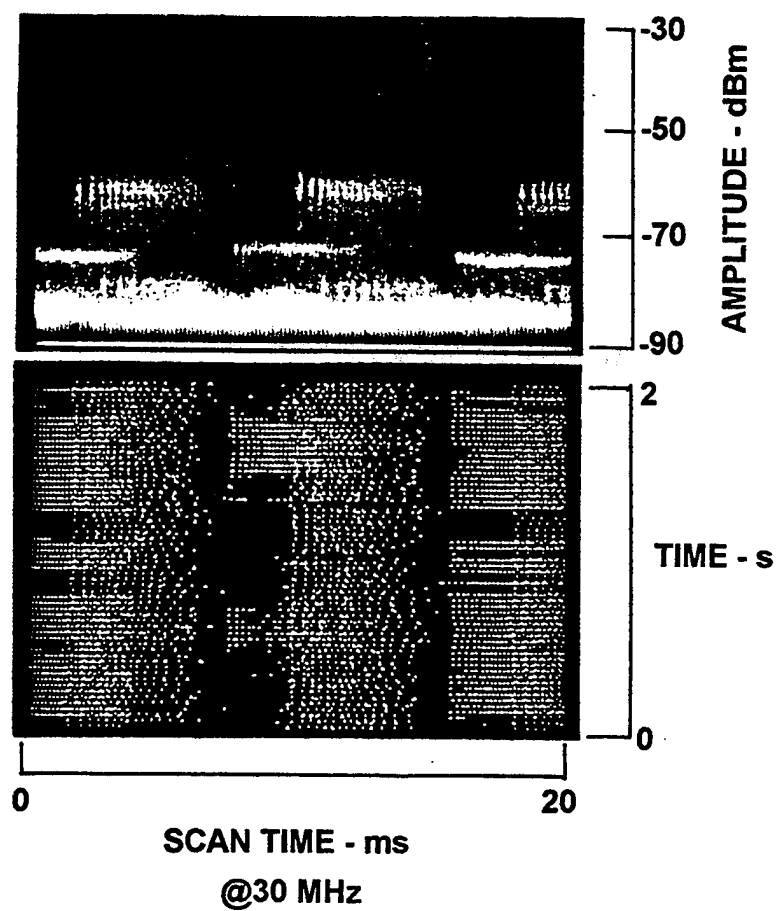
950817 0910
 HAN, RFD, LB 000
 2.9 MHz, 0, 30 kHz, 20 ms LS
 BPF 9, +20, 0, -10

Figure 2.13: Classic Gap Noise Source. Structure: Regular with Unstable and Erratic Impulses.



950817 1425
 HAN, RFD, LB 096
 3.5 MHz, 0, 30 kHz, 20 ms
 BPF 9, +20, 0, -20

Figure 2.14: Classic Gap Noise Source. Two Sources. One Source is Active on Only One Half-cycle and is also Intermittent.



951026 1354
DET-J, LP A1H
30 MHz, 0, 300 kHz, 20 ms LS
F_{36.5}, 0, 0, -10

Figure 2.15: Multiple Classic Gap Noise Sources. Three Sources.

where, T is the width of a generic gap discharge impulse, and A_p is the pulse amplitude. Figure 2.16 represents the pulse shape.

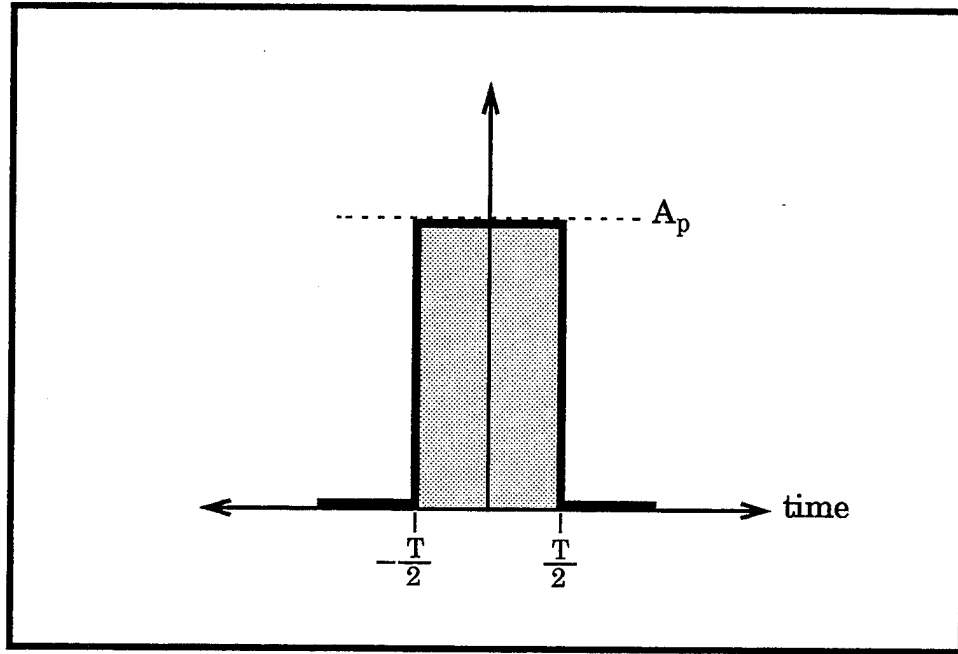


Figure 2.16: Ideal Square Pulse.

Using Fourier analysis we can decompose the spectral components of a nonperiodic waveform. The Fourier transform of $x(t)$ is given by

$$X(f) = \mathfrak{F}[x(t)] = \int_{-\infty}^{\infty} x(t) e^{-j2\pi ft} dt \quad (2.9)$$

Now, applying the transform to $x(t)$, we get

$$\begin{aligned} X(f) &= \int_{-\infty}^{+\infty} x(t) e^{-j2\pi f\tau} d\tau \\ &= \int_{-\frac{T}{2}}^{\frac{T}{2}} A_p e^{-j2\pi f\tau} d\tau \end{aligned} \quad (2.10)$$

If we let $u = -j2\pi f\tau$, and $du = -j2\pi f d\tau$, then substitute into eq. 2.10 we get

$$\begin{aligned}
X(f) &= \frac{A_p}{-j2\pi f} \int_{-\frac{T}{2}}^{\frac{T}{2}} e^u du \\
&= \frac{A_p}{-j2\pi f} \left[e^{-j2\pi f \tau} \right]_{-\frac{T}{2}}^{\frac{T}{2}} \\
&= \frac{A_p}{-j2\pi f} \left[e^{-j2\pi f \left(\frac{T}{2}\right)} - e^{-j2\pi f \left(-\frac{T}{2}\right)} \right] \\
&= \frac{A_p}{\pi f} \left[\frac{e^{j\pi f T} - e^{-j\pi f T}}{j2} \right]
\end{aligned} \tag{2.11}$$

By applying Euler's identity, $\sin(\alpha) = \frac{e^{j\alpha} - e^{-j\alpha}}{j2}$, and multiplying by $\frac{T}{T}$ we get

$$\begin{aligned}
X(f) &= A_p T \left[\frac{\sin(\pi f T)}{\pi f T} \right] \\
&= A_p T \text{sinc}(\pi f T)
\end{aligned} \tag{2.12}$$

We see that a square pulse in the time domain transforms to the sinc function in the frequency domain. The width of a pulse determines the nulls of the sinc function spectral lobes with a $1/T$ relationship.

Beasley [Ref. 6] measured spark impulse waveforms in a controlled laboratory setting. The basic conditions were a 60-Hz, 6-kV source applied across a 0.030 inch spaced cast steel electrode gap. His experiment demonstrated a gap discharge impulse to have a main lobe approximately 3 nanoseconds (ns) wide. The impulse continued to decay until it was insignificant at approximately 6 ns. Figure 2.17 plots Eq. 2.12 for two different pulse widths: 3 ns, and 6 ns. All other conditions are the same. Notice that a narrow duration pulse produces an ultra-wideband spectrum. Furthermore, the main lobe of each sinc function spans hundreds of megahertz—well into the VHF radio

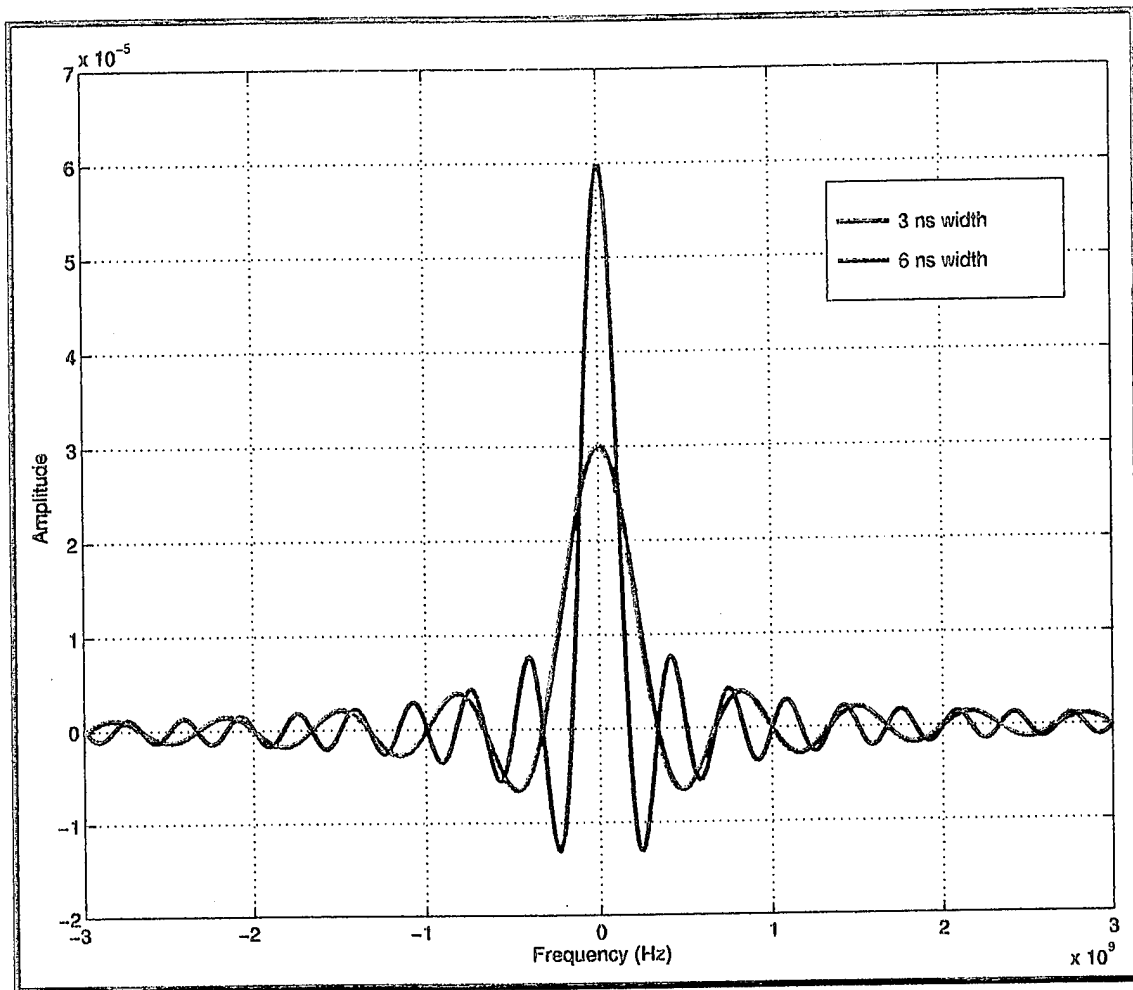
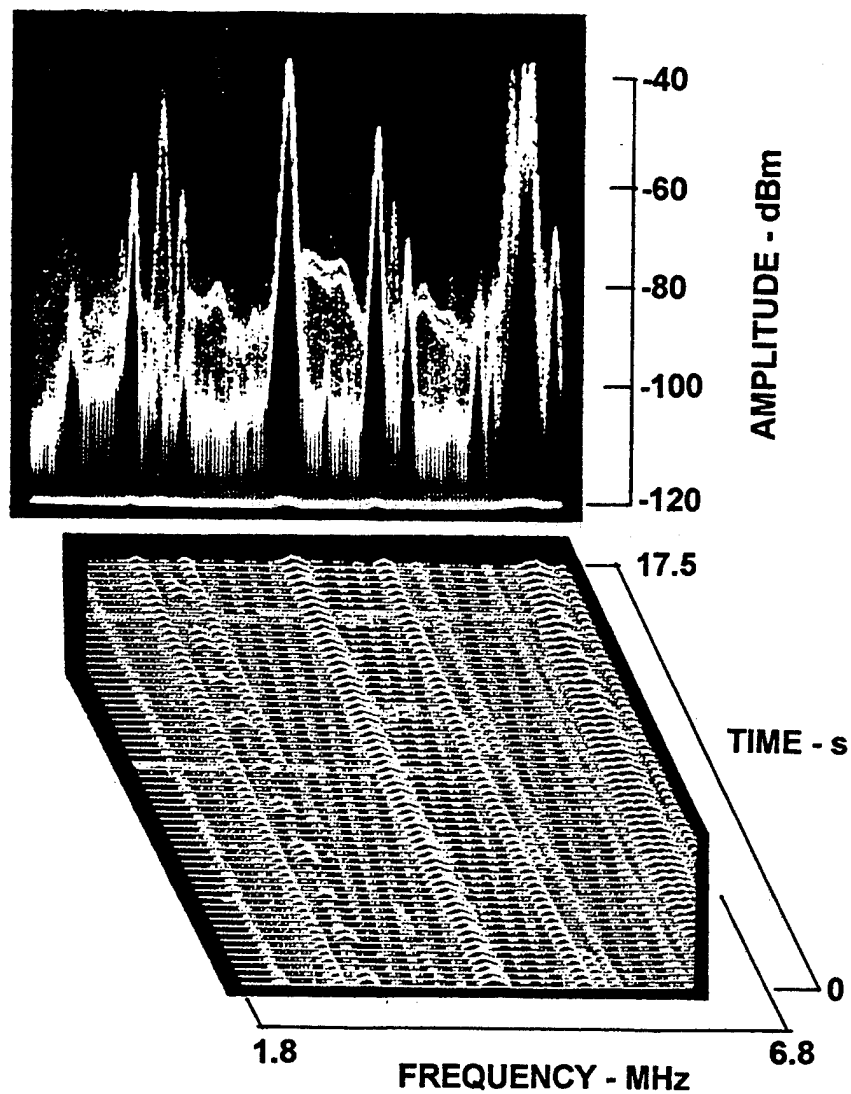


Figure 2.17: Plot of the Sinc(x) Function.

band. If one views Figure 2.17 and considers that a classic gap noise source will likely generate numerous different width impulses, one can infer that a significant portion of the frequency spectrum can be affected by one active source.

A gap breakdown discharge is a complex non-linear process. The non-linear processes that exist support interaction, or modulation, between the fundamental power-line frequency and the ultra-wideband frequency spectra generated through an impulsive gap breakdown discharge. The effect of this interaction can also be understood by applying the frequency shifting property of the Fourier Transform to the fundamental power-line frequency (and its

harmonics) and the generated sinc functions. The impact that this relationship has can be seen in Figure 2.18. This figure shows the effect, in the frequency domain, of the gap discharge source displayed in Figure 2.8. The lines that run diagonal across the lower picture represent the 60-Hz fundamental power-line frequency. The 60-Hz has been translated throughout the HF spectrum via mixing with the ultra-wideband spectrum of a classic gap discharge impulse.



950620 1025
 WIN, RFSS, LB 072
 4.3 MHz, 5 MHz, 30 kHz, 200 ms
 BPF 9, +20, 0, -20

Figure 2.18: Frequency Domain Effect of Gap Discharge Source Shown in Figure 2.8.

III. MAN-MADE NOISE PREDICTION CURVES

A. INTRODUCTION

The International Radio Consultative Committee (CCIR) generates numerous reports concerning radio communications. Three of these reports, CCIR Report 258, CCIR Report 322, and CCIR Report 670, are applicable to this investigation.

The focus of each of these reports is to predict the ambient radio frequency noise level within a specific category. The predicted noise level can then be used to establish baseline environmental noise characteristics of a location or to determine the performance of a specific radio communications system if placed at that location.

The principle metric in the CCIR reports is the noise figure, F_a , in decibels, for a short (9 ft) vertical lossless antenna over a perfectly conducting ground plane. The noise figure is derived from the corresponding noise factor, f_a , which is defined throughout each report as:

$$f_a = \frac{p_n}{kT_o b} \quad (3.1)$$

where, p_n is the noise power available from an equivalent loss-free antenna (W), k is Boltzmann's constant $= 1.38 \times 10^{-23}$ (J/K), T_o is the reference temperature, taken as 288 K, and b is the effective receiver bandwidth (Hz). [Ref. 3]

B. CCIR REPORT 258: MAN-MADE RADIO NOISE

The work of Spaulding and Disney [Ref. 19] provides the substance of CCIR Report 258 [Ref. 20]. The radio noise level prediction schema of this report is based on the environmental category in which the receive antenna is

located. The environmental categories, are: business, residential, rural, and quiet rural.

Business areas are defined as any area where the predominant usage throughout the area is for any type of business (e.g. stores and offices, industrial parks, large shopping centres, main streets or highways lined with various business enterprises, etc.). Residential areas are defined as any area used predominately for single or multiple family dwellings with a density of at least five single family units per hectare [10,000 sq. meters] and no large or busy highways. Rural areas are defined as areas where dwellings are no more than one every two hectares. ...quiet rural areas) corresponds to the values of man-made noise at carefully selected quiet receiving sites as reported in Report 322. [Ref. 1]

Spaulding and Disney [Ref. 19] provide further guidance on how to interpret the environmental categories:

The residential area is defined here as any area used predominately for single or multiple family dwellings with a density of at least two single family units per acre and no large or busy highways. An occasional isolated business such as a drugstore or filling station can be included, but a city block or more of concentrated business enterprises should be considered a business area. This definition applies to both urban and suburban residential areas. Rural areas are defined here as locations where land usage is primarily for agricultural or similar pursuits, and dwellings are no more than one every five acres.

Measurements recorded throughout the United States of America during 1966 to 1971 form the basis for the prediction curves. With the exception of a few stationary measurements conducted on the grounds of the Department of Commerce Boulder Laboratories (Colorado), the bulk of the data was obtained using a mobile noise measurement laboratory. [Ref. 19]

The mobile laboratory consists of a tractor and a van. The tractor utilizes a full diesel engine and was purchased under the MIL-specifications for a quiet vehicle. Additional noise suppression was added after delivery; e.g., suppression on windshield wiper motor, alternator and controls, wheel bearings, etc. A diesel generator set was installed between the cab and the fifth wheel to provide power for mobile or remote operation. A

low-boy type semitrailer van is used so that a two-meter-high vertical antenna on the van roof will clear power and telephone lines that might be encountered during mobile measurements. The van has an exterior aluminum skin with the roof acting as the ground plane for the receiving antennas. [Ref. 19]

All non-stationary measurements were conducted in the pre-noon hours. Figure 3.1 is a plot of the linear variation (F_{am}) of the median values of man-made noise power expressed in terms of F_a (dB above thermal noise at $T_0 = 288$ K). Where $F_{am} = c - d \log f$, with f expressed in MHz and c and d corresponding to the values listed in Table 3.1 in the appropriate environmental category. The galactic noise information is provided for comparison. [Ref. 1]

Table 3.1: Values of constants c and d .

Environmental category	c	d
Business	76.8	27.7
Residential	72.5	27.7
Rural	67.2	27.7
Quiet Rural	53.6	28.6
Galactic noise	52.0	23.0

Based on a comparison difference between data collected in the United States of America and in the United Kingdom CCIR Report 258 suggested that differences in patterns of electrical and mechanical appliance utilization can lead to differing values of man-made noise power. This point will be discussed further in Chapter VI. [Ref. 1]

C. CCIR REPORT 322: CHARACTERISTICS AND APPLICATIONS OF ATMOSPHERIC RADIO NOISE DATA

This report characterizes atmospheric (due to lightning) noise levels on a global scale. Sixteen stations around the world collected data during the

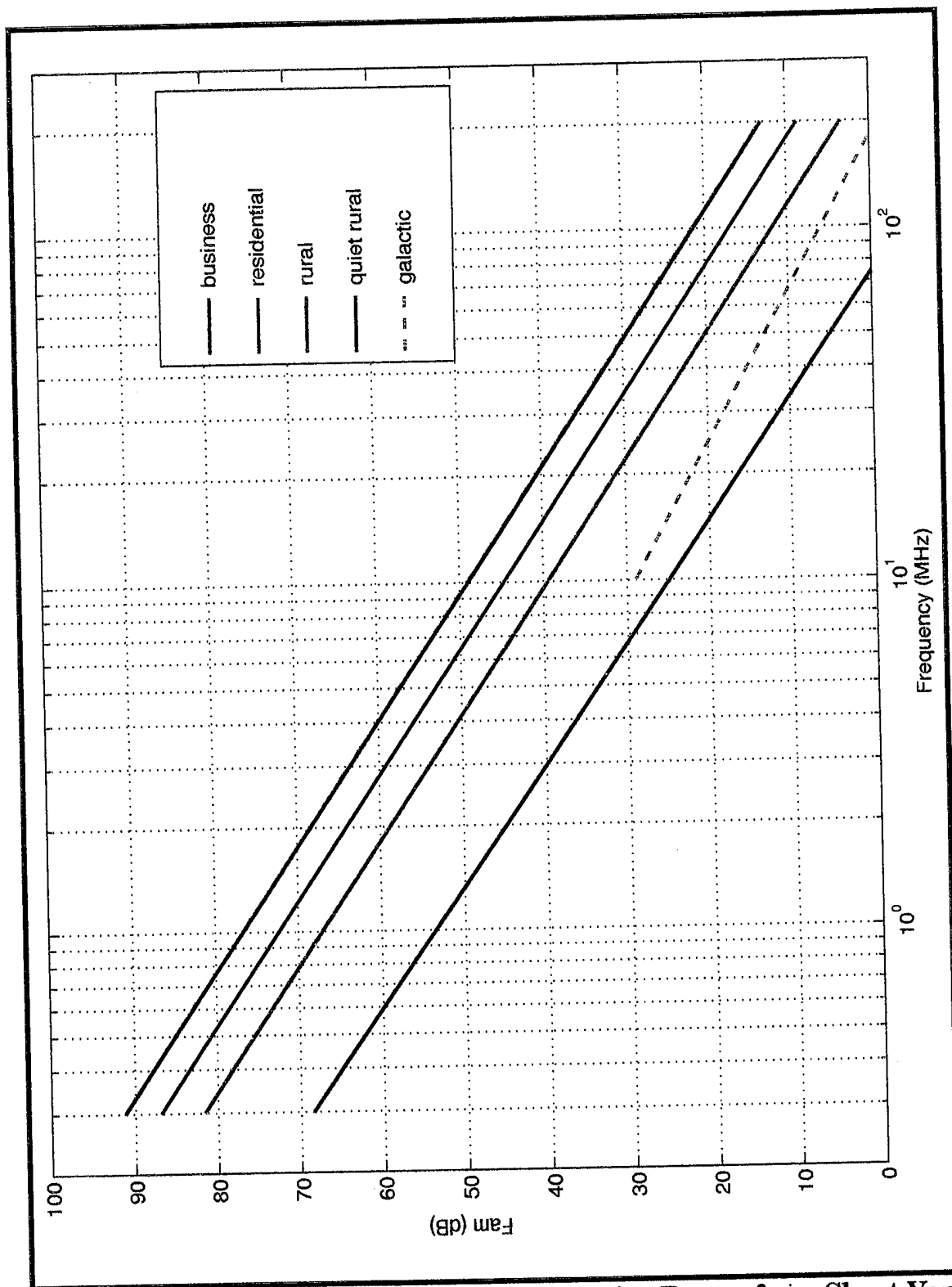


Figure 3.1: Median Values of Man-made Noise Power for a Short Vertical Lossless Grounded Monopole Antenna. After Ref. [1].

period 1957 to 1966 inclusive. The effects of man-made noise and unwanted signals were removed from the data prior to analysis. The main parameter presented is the median hourly value of the average noise power of each "time block." Table 3.2 demonstrates how a time block is formed. Each year was

Table 3.2: CCIR Report 322 Time Block.

Time Block				
a collection over one season of the same four hour time slot				
Day 1	Day 2	...	Day 89	Day 90
0000-0400	0000-0400	...	0000-0400	0000-0400
0400-0800	0400-0800	...	0400-0800	0400-0800
0800-1200	0800-1200	...	0800-1200	0800-1200
1200-1600	1200-1600	...	1200-1600	1200-1600
1600-2000	1600-2000	...	1600-2000	1600-2000
2000-2400	2000-2400	...	2000-2400	2000-2400

divided up into four seasons of approximately 90-days length. Each day of a season was divided into six, four hour time periods. Using this scheme each season generated six different time blocks. Within a time block the four hour daily period was divided up into hourly increments. During each hour the noise power was sampled on eight different frequencies for 15 minutes each. From these samples the median hourly value of the average noise power for each time block is derived. The data was combined and the results presented on one frequency, 1 MHz. The means of obtaining the 1-MHz result are described in Spaulding and Washburn [Ref. 18]. [Ref. 3]

The "quiet rural" noise levels of CCIR Report 258 were derived from analysis of the CCIR Report 322 data. Although the "quiet rural" locations are not specifically detailed in this report, the data for a "quiet receiving" location is mentioned as coming from the same sites that were selected to collect

the atmospheric noise data. The ambiguity in location description and parameters hampers further analytical discussion of "quiet rural" areas in this thesis. [Ref. 1, 3]

D. CCIR REPORT 670: WORLDWIDE MINIMUM EXTERNAL NOISE LEVELS, 0.1 HZ TO 100 GHZ

A problem that hinders the direct analysis, from prediction curves, of the effect of noise to a communications receiver arises when the type of antenna utilized on the CCIR noise measurement system differs from the type of antenna utilized with the communication system.

The measurements conducted in support of CCIR reports are generally performed using short grounded vertical monopole antennas. This type of antenna is not typically used to collect a SOI. According to CCIR Report 670 [Ref. 21], "The majority of the results... are for omni-directional antennas.... The average value of F_a for directional antennas will be the same if random direction is assumed."

It is the opinion of the author that the notion of randomly directing a directional antenna for the purpose of extracting pertinent noise power data is of no practical value to the communicator and should be disregarded. It is the belief of the author that a receiving site will use an antenna, applied in a specific direction, with the intention of utilizing it for a non-random application. And, even though, the direction of the antenna may vary in azimuth, it will remain stationary for an extended observation period before moving to another azimuth. Consequently, it is what the antenna "sees" during the extended observation period that must be accounted for—not the culmination of random directions. One additional factor must be considered. The dominant sources of man-made radio noise are low in numbers and from discrete locations. They are not randomly distributed. The sources can be located and mitigated.

IV. POWER-LINE NOISE FIELD MEASUREMENTS

Appendix A describes the instrumentation and data-collection method. Appendix B describes the data-collection locations.

A. INTRODUCTION

Three types of classic gap-type noise data were collected at seven sites around the world: the temporal structure (presented in Chapter II), the amplitude-versus-frequency, and the amplitude-versus-receiver bandwidth. The data used in this investigation was limited to representing gap-type discharges; i.e. data collected during this investigation that contained motor-controller noise, uninterruptable power supply noise, RF arc-welder noise, and other similar power-line radiated noise processes was not incorporated in the data presented in this thesis since they were too erratic to place into a measurable category.

The amplitude-versus-frequency data for all plots have been adjusted (see Section D of this chapter) to a 30-kHz receiver bandwidth. The data points for the plots contained in the figures of this chapter were extracted from 51 photographs of 3-axis time-history spectral-band displays. The method used to extract data points from a photograph was to overlay the photograph with a fine-scale translucent vellum grid and record the noise amplitude in terms of the grid line number and its corresponding spectral grid line number. The grid lines were then scaled according to the photograph parameters recorded when the photograph was taken. In cases where a signal was stronger than the adjacent power-line noise, the data point was interpolated from the levels of power-line noise on either side of the signal bounds.

B. FREQUENCY RANGE: 2 - 8 MHZ

Figure 4.1 displays data measurements in the 2- to 8-MHz range. This figure incorporates data from four different geographical locations. The three-digit number following each legend entry corresponds to the antenna azimuth of the data. The gap discharge noise source of Figure 2.7 generated the spectral distribution of WIN LB 048. The source (see Figure 2.8) for WIN LB 072 was precisely located and had a 1.13 km line-of-sight distance. The source (see Figure 2.9) for WIN LB 108 was precisely located and had a 0.62-km line-of-sight distance. The source for HAN LB 072 was precisely located and had a 1.36-km line-of-sight distance. The source (see Figure 2.13) for HAN LB 000 was precisely located and had a 0.9-km line-of-sight distance.

C. FREQUENCY RANGE: 10 - 50 MHZ

Figure 4.2 displays data measurements in the 10- to 50-MHz range.

D. FREQUENCY RANGE: 0 - 235 MHZ

Figure 4.3 displays data measurements in the 0- to 235-MHz range.

E. AMPLITUDE VERSUS BANDWIDTH

The amplitude-versus-receiver bandwidth measurement was conducted at three locations comprising 20 measurements (13 taken from the 2.0 to 8.0 MHz range and seven taken from 30 to 215 MHz). The method utilized was to locate a classic gap noise source on an antenna azimuth, then visually scan the frequency band for areas that had no signals present (they would corrupt the measurements). Once an area was isolated, the spectrum analyzer was switched to the single-frequency mode and the bandwidth measurements

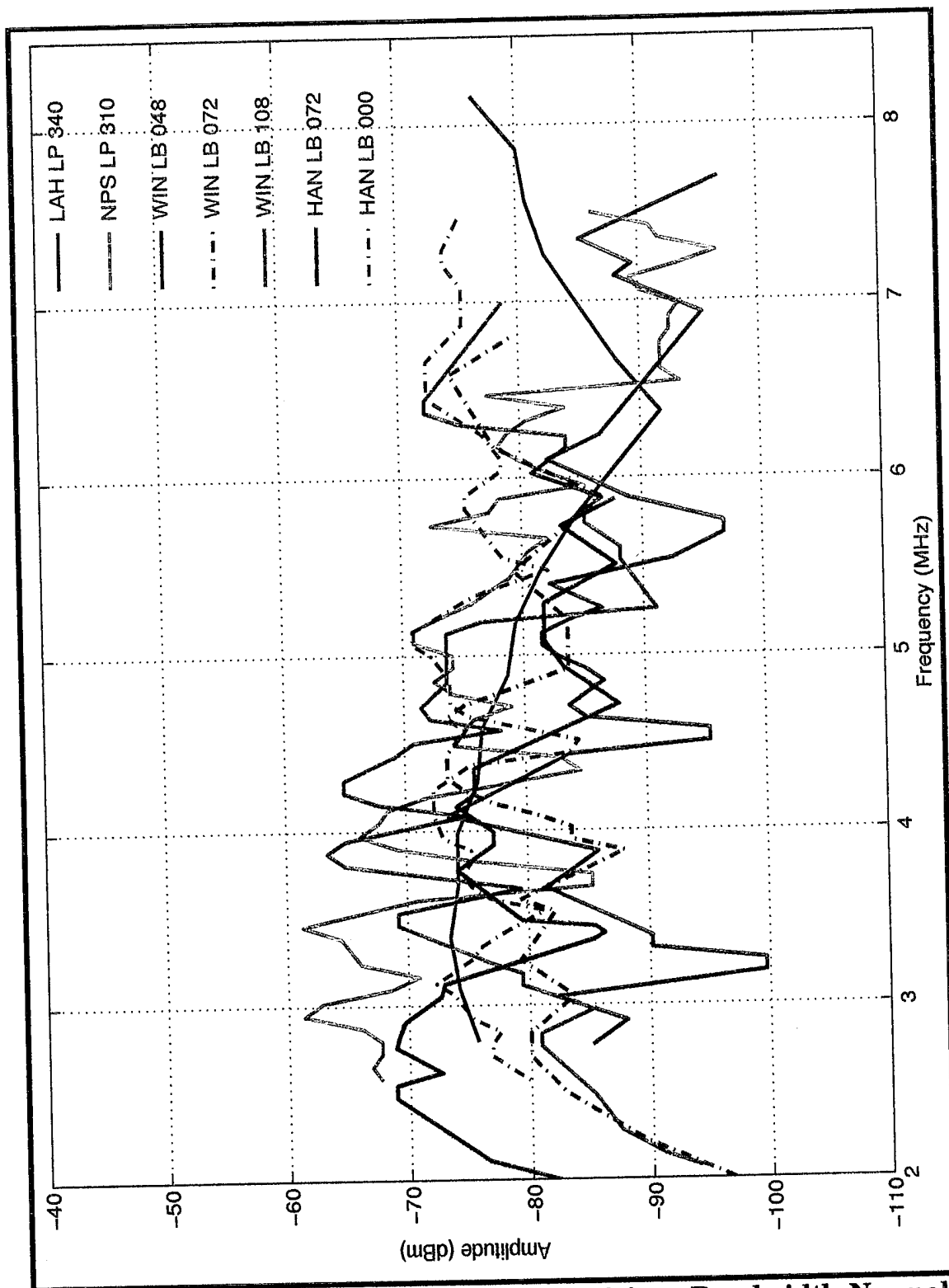


Figure 4.1: Classic Gap-type Power-line Noise. Bandwidth Normalized to 30 kHz. Frequency Range: 2 to 8 MHz.

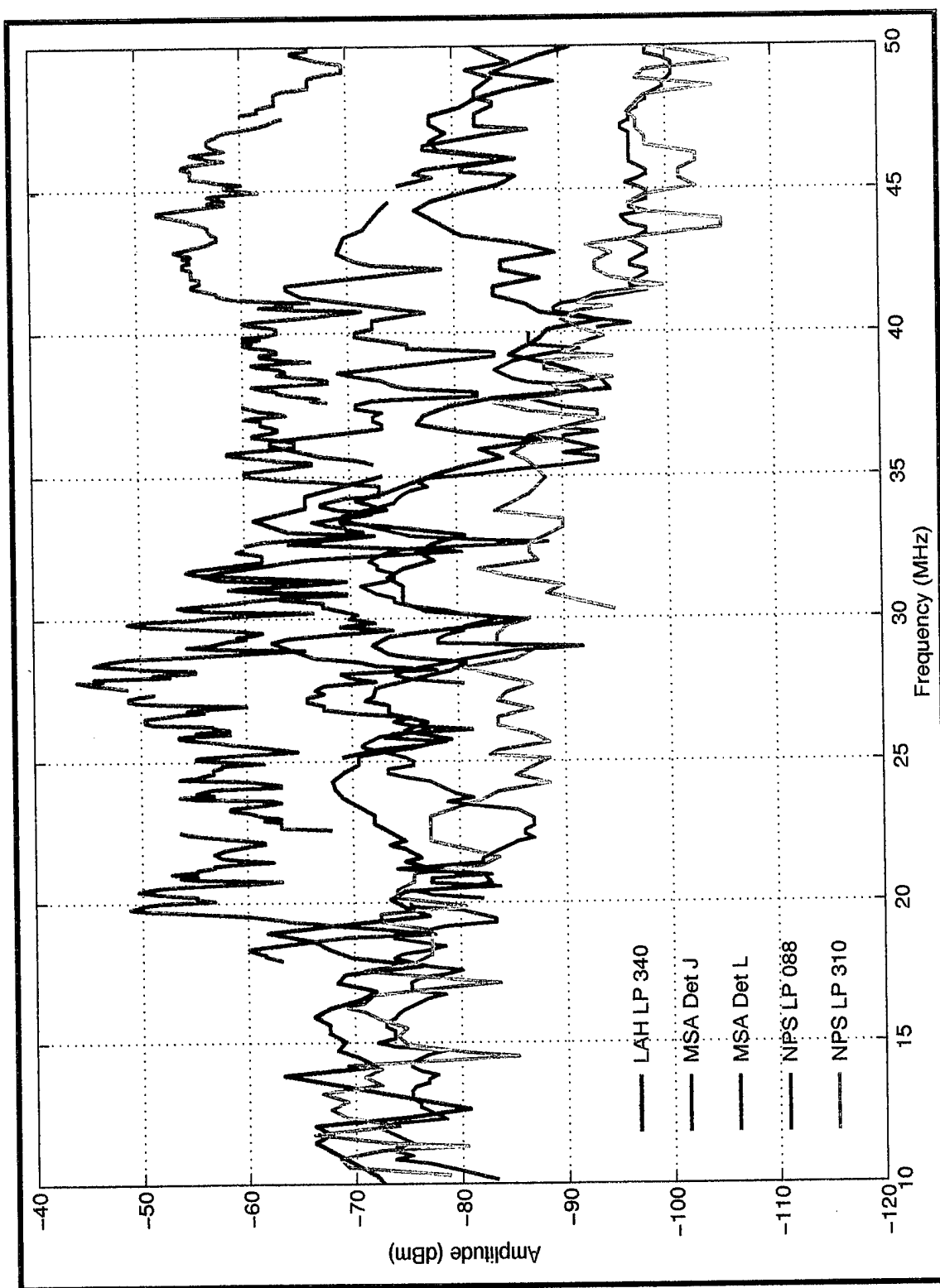


Figure 4.2: Classic Gap-type Power-line Noise. Bandwidth Normalized to 30 kHz. Frequency Range: 10 to 50 MHz.

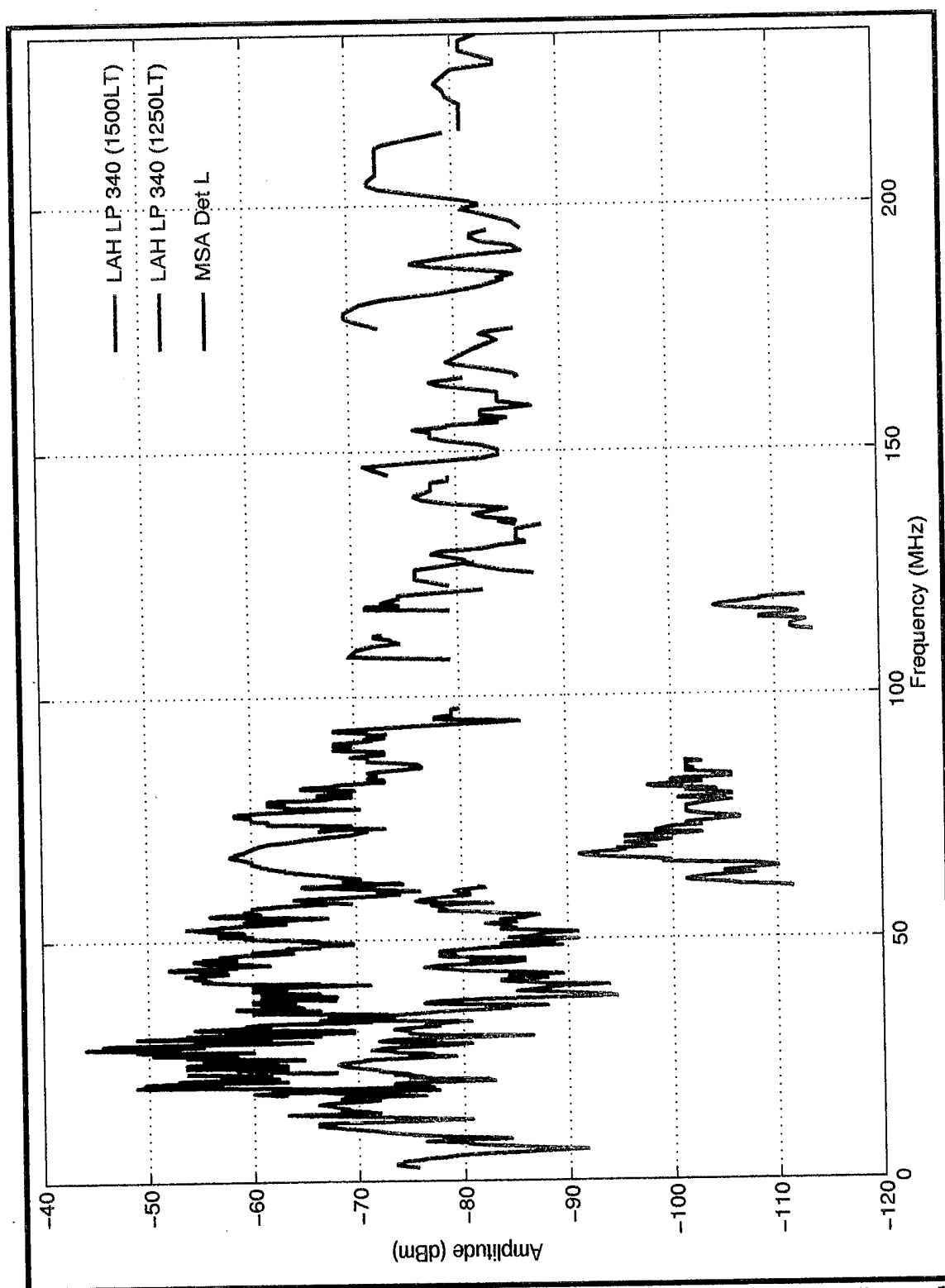


Figure 4.3: Classic Gap-type Power-line Noise. Bandwidth Normalized to 30 kHz. Frequency Range: 0 to 235 MHz.

recorded. The data for each location was normalized relative to the 3-kHz measurement then averaged according to bandwidth. The results are presented in Figure 4.4. This figure highlights a trend in the data. The normalized amplitude-versus-bandwidth characteristics of gap-type noise sources can be considered independent of signal frequency, geographical location, or environmental category.

Using the results displayed in Figure 4.4, the mean value from each location was averaged with the other locations according to bandwidth. The results are displayed in Figure 4.5 and the numeric values listed in Table 4.1.

Table 4.1: Average Mean for Amplitude versus Bandwidth.

Bandwidth (kHz)	3	10	30	100	300
Average Mean	0.0	10.2	19.7	30.1	37.1

Using the values in Table 4.1, a bandwidth measurement adjustment matrix was developed. Table 4.2 lists the adjustment values. To apply the

Table 4.2: Bandwidth Measurement Adjustment Matrix.

Bandwidth		Bandwidth of Measurement				
		3 kHz	10 kHz	30 kHz	100 kHz	300 kHz
Adjustment (dBm) when converting to:	3 kHz	0.0	-10.2	-19.7	-30.1	-37.1
	10 kHz	+10.2	0.0	-9.5	-19.9	-26.9
	30 kHz	+19.7	+9.5	0.0	-10.4	-17.4
	100 kHz	+30.1	+19.9	+10.4	0.0	-7.0
	300 kHz	+37.1	+26.9	+17.4	+7.0	0.0

adjustment matrix we will utilize the following example. Suppose that a man-made noise survey, utilizing a 3-kHz bandwidth receiver, was conducted at a potential receiver site. The results of the survey are presented in Table 4.3.

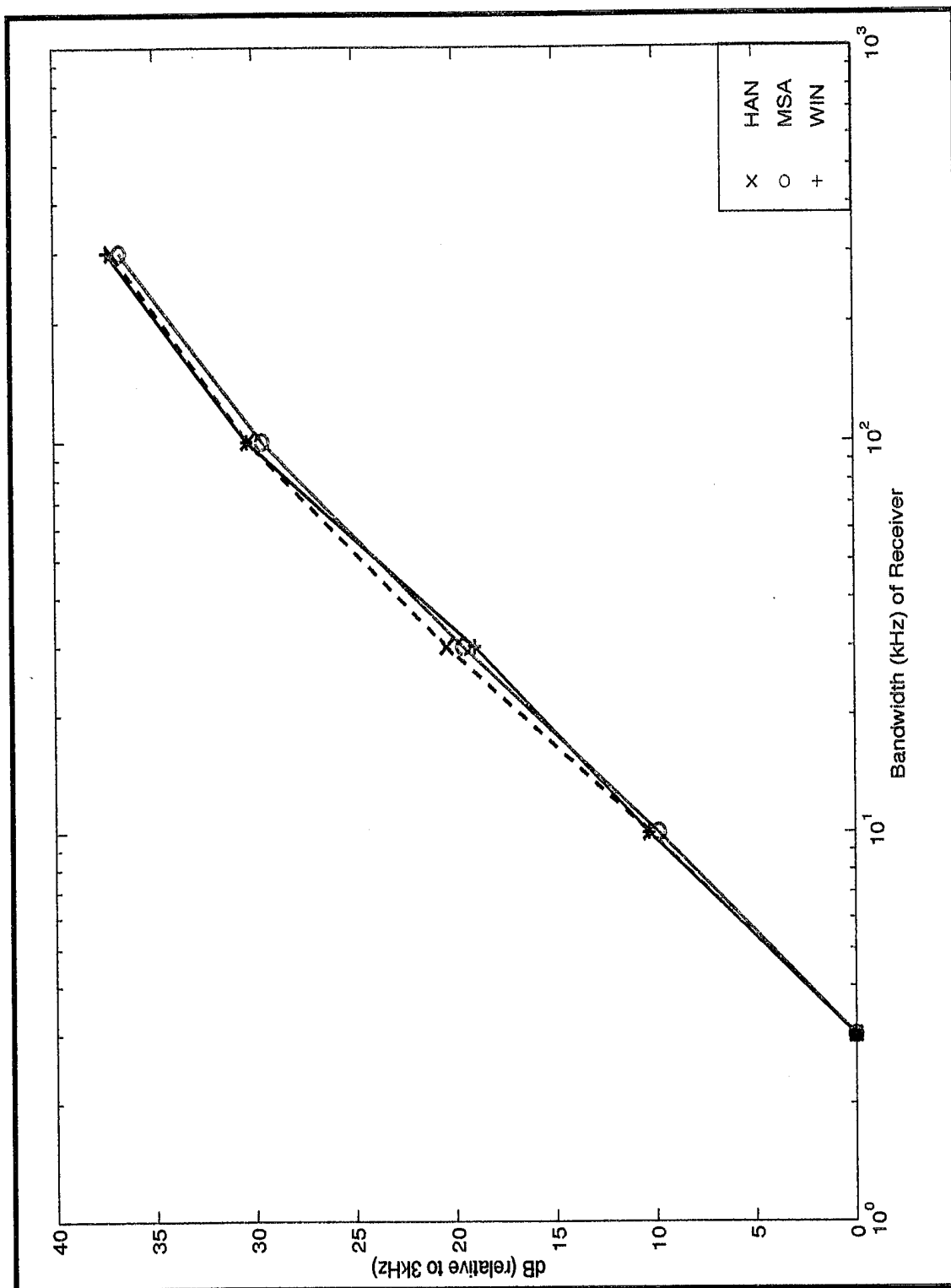


Figure 4.4: Amplitude of Power-line Noise as a Function of Receiver Bandwidth (all data has been reduced and normalized to 3 kHz).

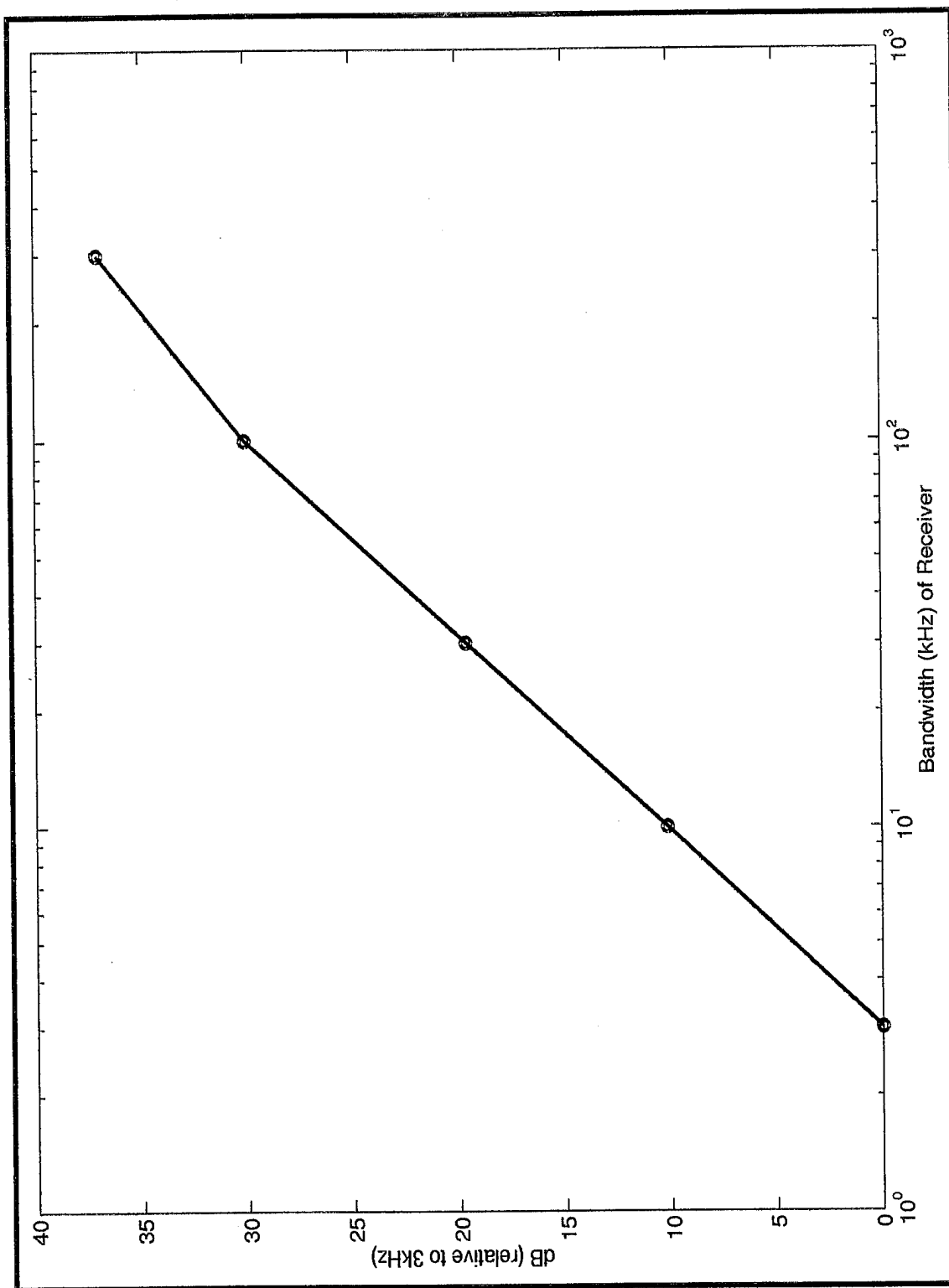


Figure 4.5: Average of the Mean Amplitude versus Bandwidth Data for 20 Measurements Recorded at Three Geographical Locations.

To determine the noise level that a 300-kHz bandwidth receiver would experience at that site (using the same data previously collected), apply the band-

Table 4.3: Man-made Noise Survey Conducted at a Potential Receiver Site.

Frequency (MHz)	13.0	13.5	14.0	14.5
Amplitude (dBm)	-101.3	-93.8	-81.0	-88.2

width adjustment values given in Table 4.2. For this example—measurement bandwidth of 3-kHz, adjusting to a bandwidth of 300-kHz—the adjustment value is +37.1 dBm. Now, adjust the measured data by adding +37.1 dBm. The results are presented in Table 4.4.

Table 4.4: Man-made Noise Levels Adjusted for a 300-khz Bandwidth Receiver.

Frequency (MHz)	13.0	13.5	14.0	14.5
Amplitude (dBm)	-64.2	-56.7	-43.9	-51.1

V. ANALYSIS OF FIELD MEASUREMENTS

A. INTRODUCTION

The power-line noise levels recorded during the field measurements are expressed in dBm. Using the terminology of CCIR Report 670, the field measured data represents p_n , the available external noise power level. The man-made noise-level prediction curve in CCIR Report 258 is expressed in F_{am} (dB above kT_0b), where

$$F_{am} = c - d \log f \quad (5.1)$$

is calculated using the appropriate environmental category coefficients for c and d (see Chapter III, Section B). We can relate F_{am} to available external noise power by allowing

$$F_{am} = 10 \log(f_a) \quad (5.2)$$

where

$$f_a = \frac{p_n}{kT_0b}. \quad (5.3)$$

Substituting Eq. 5.3 into Eq. 5.2 and solving for p_n , we find

$$p_n = \text{INVLOG}\left(\frac{F_{am}}{10}\right) \cdot kT_0b. \quad (5.4)$$

We can express p_n , in dBm by

$$(p_n)_{dBm} = 10 \log \left(\frac{\text{INVLOG}\left(\frac{F_{am}}{10}\right) \cdot kT_0b}{1 \times 10^{-3}} \right). \quad (5.5)$$

Calculating Eq. 5.1 (using the appropriate environmental coefficients), and applying the results to Eq. 5.5, we can solve for $(p_n)_{dBm}$, and directly compare

the CCIR Report 258 predicted values to the field measured data. The CCIR prediction curve (rural) represented in the figures of this chapter was generated using Eq. 5.1 and Eq. 5.5.

B. FREQUENCY RANGE 2 TO 8 MHZ

Figure 5.1 shows the 2- to 8-MHz field data, normalized to a 30-kHz receiver bandwidth, compared to the CCIR Report 258 prediction for man-made noise in a rural environment. Notice that the slope of the totality of the receiver site data follows the slope of the CCIR prediction curve. The amplitude of the receiver site data deviates +16 dBm to -33 dBm from the CCIR curve.

C. FREQUENCY RANGE 10 TO 50 MHZ

Figure 5.2 shows the 10- to 50-MHz field data, normalized to a 30-kHz receiver bandwidth, compared to the CCIR Report 258 prediction for man-made noise in a rural environment. Notice that the totality of the field measured data follows the slope of the CCIR prediction curve. The amplitude of the receiver site data exceeds the CCIR prediction throughout the entire frequency range. The maximum deviation from the CCIR prediction is +57 dBm.

D. FREQUENCY RANGE 0 TO 235 MHZ

Figure 5.3 shows the 0- to 235-MHz field data, normalized to a 30-kHz receiver bandwidth, compared to the CCIR Report 258 prediction for man-made noise in a rural environment. Notice that the slope of both data sets (LAH and MSA) are similar to the CCIR predicted curve. The majority of all field measurements exceed the CCIR predicted values. The MSA Det L data is considerably higher than CCIR predicts.

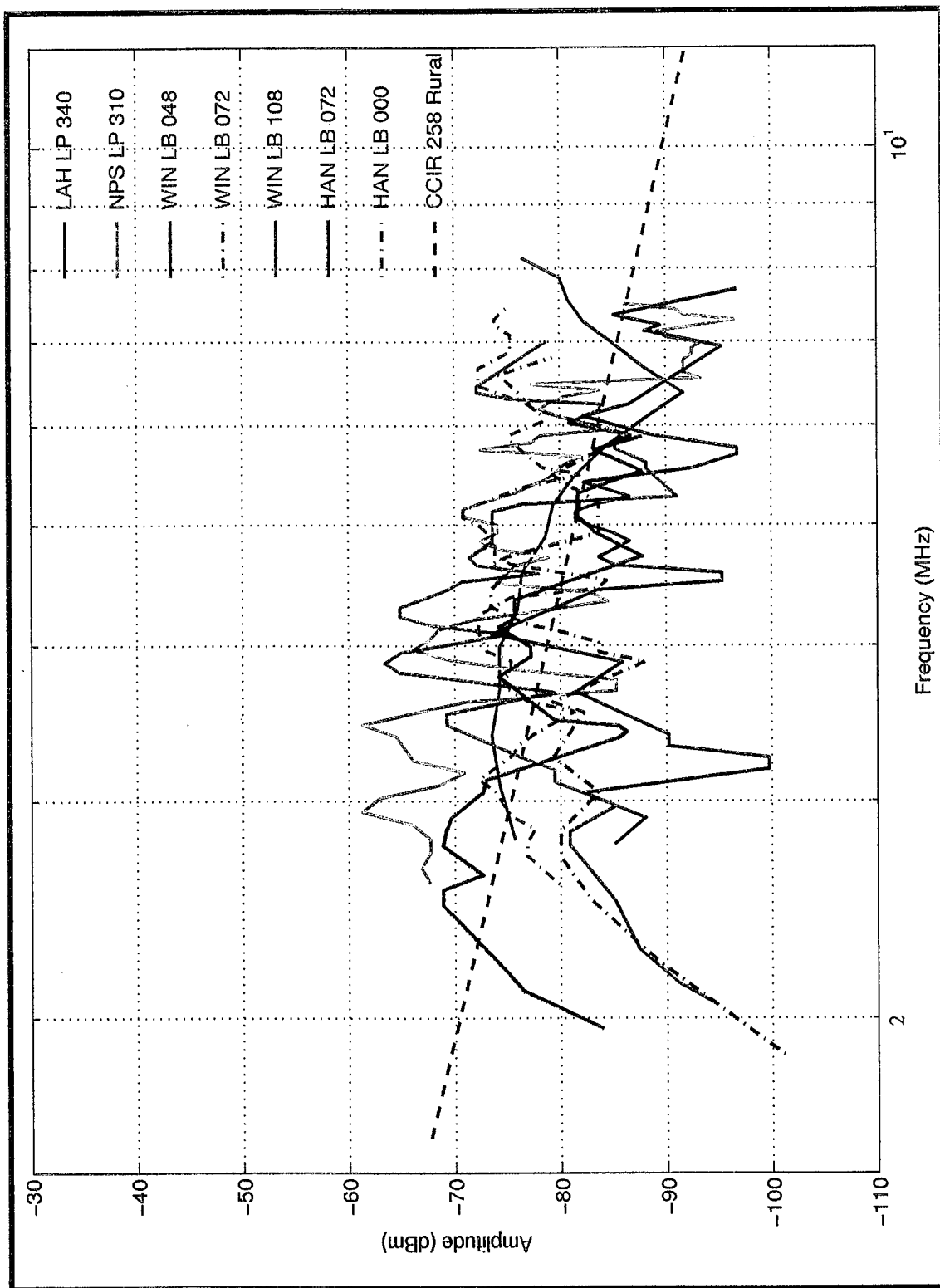


Figure 5.1: Bandwidth Normalized (30 kHz), Power-line Noise Versus CCIR 258 Prediction Curve (rural). Frequency Range: 2 to 8 MHz.

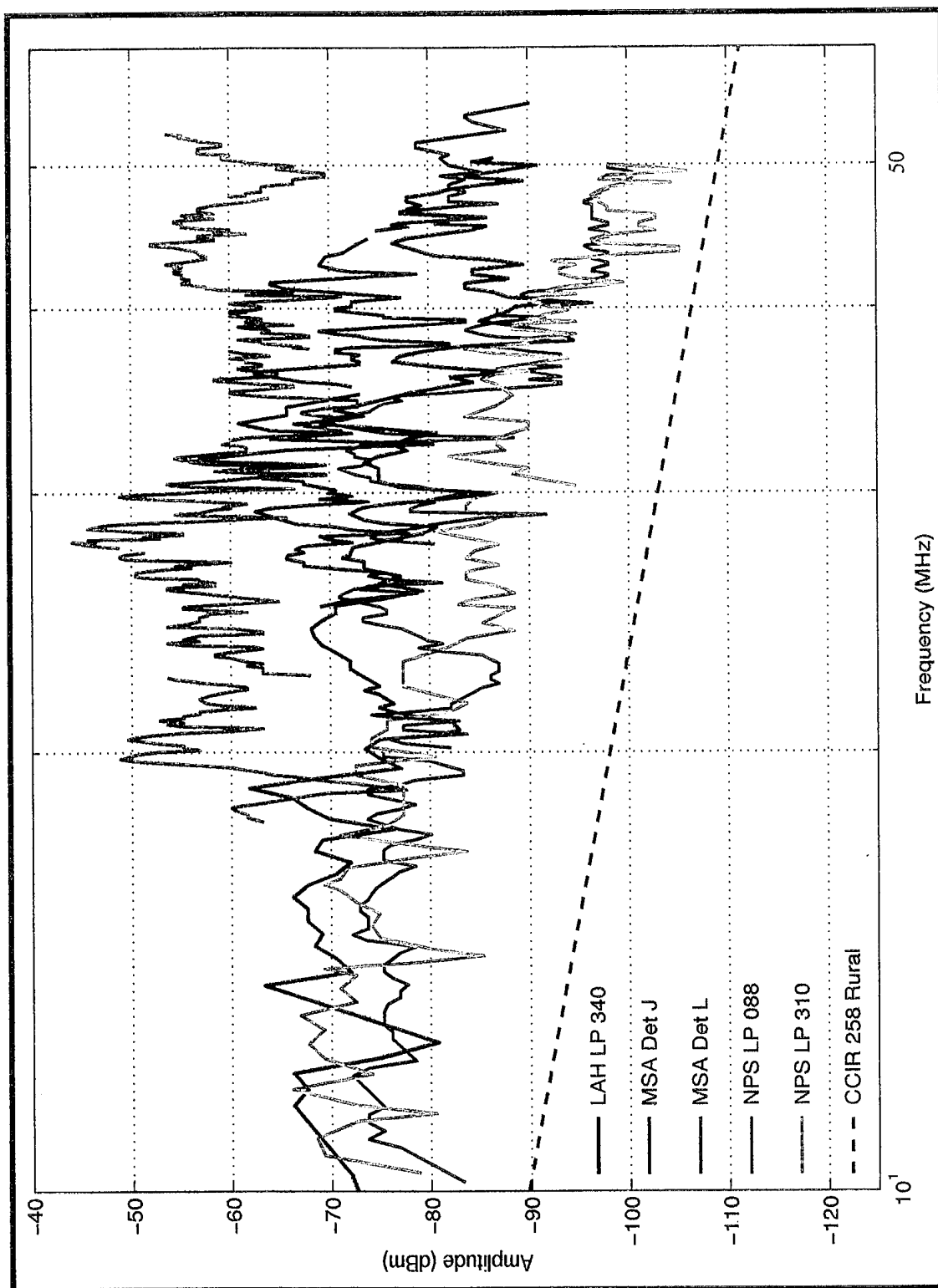


Figure 5.2: Bandwidth Normalized (30 kHz), Power-line Noise Versus CCIR 258 Prediction Curve (rural). Frequency Range: 10 to 50 MHz.

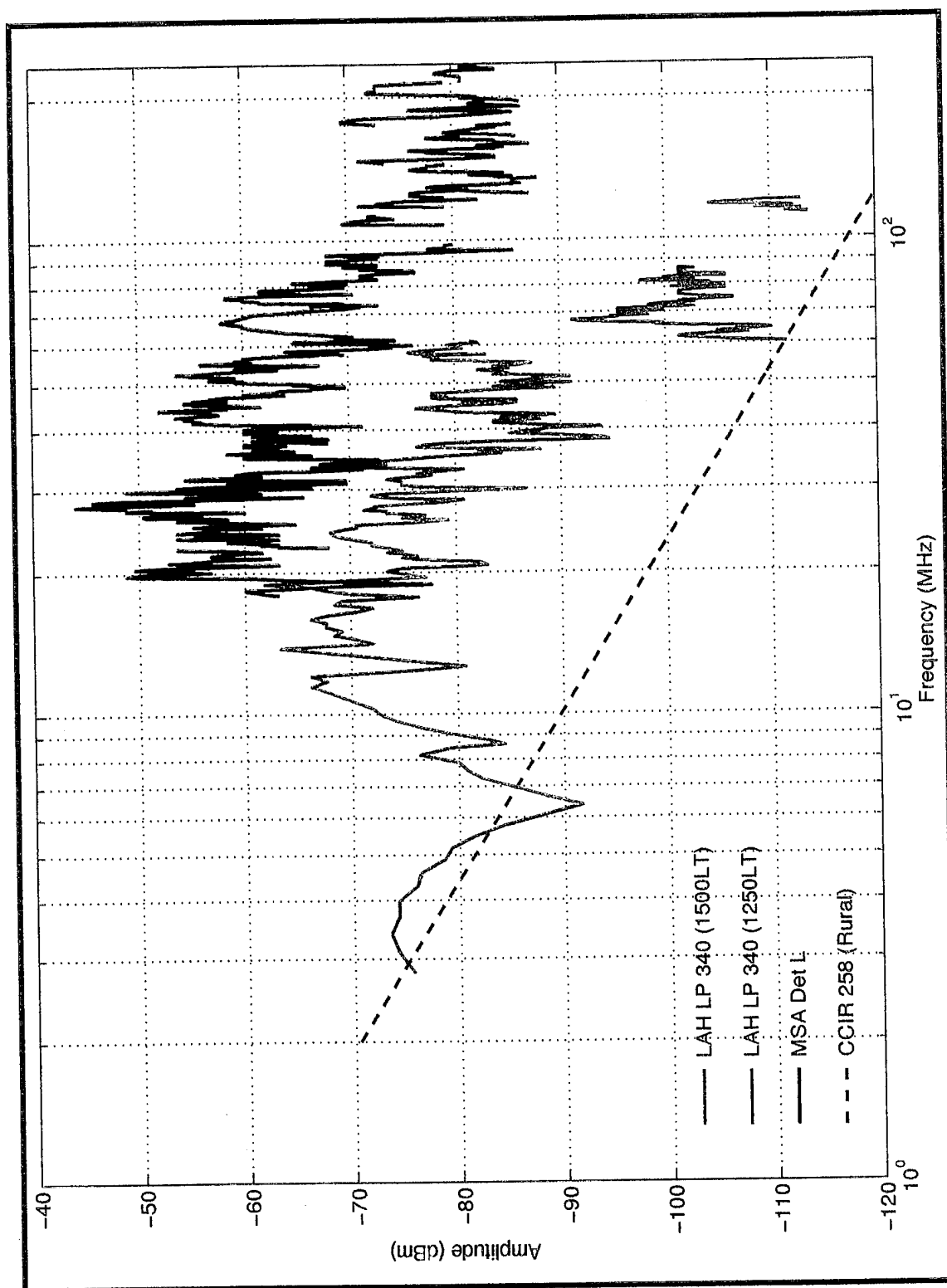


Figure 5.3: Bandwidth Normalized (30 kHz), Power-line Noise Versus CCIR 258 Prediction Curve (rural). Frequency Range: 0 to 235 MHz.

E. COMMENTS ON THE DIFFERENCES BETWEEN FIELD MEASURED DATA AND CCIR PREDICTED VALUES

The data for the CCIR Report 258 prediction curves comes from the work of Spaulding and Disney [Ref. 20]. The methodology for data collection during their investigation was to drive throughout an environmental area in a mobile noise measurement laboratory, generally in the pre-noon period. The amount of time that each run took varied from 15 minutes to over one hour. It is the opinion of the author that this provides a fundamental explanation to the differences observed between the receiver site data and the CCIR predicted values. [Ref. 19, 20]

The measurements for this investigation were taken from fixed receiver sites that used directional antennas. Therefore, any active noise sources that were present along the antenna azimuth were received. If an active noise source was strong and consistent then the recorded data reflects that condition (see MSA Det L entry; Figure 5.3).

Vincent and Munsch [Ref. 12] have pointed out that not all power-lines or power-line hardware generate radio-frequency noise. Consequently, the mobile laboratory used to collect CCIR Report 258 data, by virtue of being mobile, would not have been exposed to active noise sources to the same extent that is represented by the data in this thesis. i.e., the CCIR man-made noise prediction curves can only represent active sources that were in proximity of the mobile laboratory as it drove throughout an area. The relevance of the observations then become limited to the amount of time that the mobile laboratory actually spent near active sources.

The CCIR prediction curves are closer to field-measured data at lower frequencies than at higher frequencies because a low HF band ground wave will travel a farther distance than a high HF band (or VHF band) ground wave. As the mobile noise measurement laboratory drove throughout an area, the low-band HF noise from a gap-type discharge would travel farther from its

source than the high-band HF or VHF noise component. This probably led to more consistent (and accurate) noise-level presence in the lower HF band than in the higher HF or VHF band. Furthermore, the measurement areas during the time of this investigation most likely contain more power lines than existed during the time the CCIR data were collected. Thus, more noise sources probably exist at this time.

This explains why the CCIR man-made noise prediction curve is consistently lower, particularly at higher frequencies, than noise power data collected at a fixed receiver site. The circumstances under which the CCIR data was collected is not plausible for application to site selection of fixed site receivers.

VI. CONCLUSIONS AND RECOMMENDATIONS

A. URBANIZATION, ELECTRIC POWER CONSUMPTION, AND THE LEVEL OF MAN-MADE NOISE

The geographical variation in the level of man-made radio noise is primarily dependent upon the geographic distribution of the noise sources. Below about 10 MHz, man-made radio noise appears to correlate with density of electrical machinery and the power lines required to serve machinery. The convention has been adopted of segregating the levels of man-made radio noise into categories based on the level of urbanization in the area of measurement. [Ref. 22]

Relatively good correlation was found between power consumption in an area and the radio noise power below 20 MHz. [Ref. 19]

The material presented in this thesis suggests that for an environmental area neither the level of urbanization nor the power consumption is a satisfactory predictor of the man-made noise level that will exist in that area. Chapter II outlines the mechanism behind a gap-type breakdown discharge—it is primarily a function of the difference of potential across a gap—not power consumption. When the difference of potential exceeds the gap breakdown threshold a spark or microspark is generated that produces radio-frequency noise that extends into the Gigahertz range.

Vincent [Ref. 13] has suggested that the number of overhead electric power utility poles (not solely the urbanization level), in the line-of-sight vicinity of a potential receiver site would be a more accurate predictor of the level of man-made noise that could be anticipated for that site. The idea is based on the more power-line poles that exist in proximity of a receiver site, the higher the probability that there will be active gap-type noise sources. The results of

40 site surveys conducted by Vincent are listed in Table 6.1. Four of the 40 sites are duplicate surveys. They are listed independently because a successful power-line noise-mitigation effort significantly reduced the man-made noise level at each site. All sites fit the CCIR Residential or CCIR Rural environmental category.

Table 6.1: Power-line Noise Level Survey

Power-line noise level	CCIR Business	CCIR Residential	CCIR Rural	CCIR Quiet Rural
Area has MANY overhead power-lines				
None	0	1	0	0
Low	0	0	0	0
Modest	0	1	2	0
Major	0	6	11	0
Area has FEW overhead power-lines				
None	0	0	2	0
Low	0	0	3	0
Modest	0	0	5	0
Major	0	0	5	0
Area has NO overhead power-lines				
None	0	0	4	0
Low	0	0	0	0
Modest	0	0	0	0
Major	0	0	0	0

The results presented in Table 6.1 support the suggestion by Vincent that the man-made noise level of an area can be predicted more accurately by considering the number of electric power utility poles that are in the line-of-sight vicinity of the area than by placing the area in an environmental

category. Consequently, it is the recommendation of this author that the number of overhead power-line poles in the vicinity of a potential receiver site be used to initially predict the level of man-made noise level present.

A plausible basis for a more appropriate model appears to be as follows. The "no power-line" category should apply if there are no overhead power-lines within 10-km of the receiver site; the expected man-made noise level would be none. The "few power-line" category should apply if there exist no more than two overhead power-lines within 10-km of the receiver site; the expected man-made noise level would be low to modest. The "many power-line" category should apply if three or more overhead power-lines within 10-km of the receiver site; the predicted man-made noise level would major. [Ref. 13]

B. RECOMMENDATION CONCERNING THE USE OF CCIR REPORT 258

Referring back to the discussion of Chapter V, Section E, it is the recommendation of the author that CCIR Report 258 not be used to predict the man-made noise level at a potential receiver site. The recommendation presented in Section A of this chapter should be used instead.

Future measurements of man-made noise levels should be pursued to update the model presented in CCIR Report 258. It is the recommendation of this author that the existing environmental categories be replaced with categories based on the quantity of overhead power-lines.

C. MITIGATION OF POWER-LINE NOISE

A receiver site plagued by power-line noise can take action to successfully mitigate the noise sources. The *Signal-to-Noise Enhancement Program Power-Line Noise Mitigation Handbook* [Ref. 12] is an excellent resource for

such work. It provides a step-by-step procedure to locate, identify, and mitigate the sources of power-line noise. The rewards of instituting such a program are fully realized when a noisy receiver site is transformed into a noise-quiet receiver site.

The gaps that are associated with the power-line noise presented in this thesis can occur via wind action on power-line hardware, ongoing exposure fostering oxide formation, damage from lightning strikes, and through routine line-maintenance actions performed by utility companies. Consequently, the reader is cautioned to observe the comments of Lauber [Ref. 23],

An otherwise good site may be degraded intermittently, and thus checking should be done often and carefully if low radio-noise levels are to be maintained.

It is the recommendation of the author that a receiver site employ the methods outlined in Ref. 12 to mitigate existing power-line noise and that a routine evaluation of the site noise level be instituted to ensure new noise sources are located and corrected in a timely manner.

APPENDIX A. INSTRUMENTATION

The instrumentation utilized to record field measurements of the time and spectral properties of power-line noise is described in this appendix.

A. MEASUREMENT SYSTEM

Figure A.1 is a block diagram of the typical field data measurement set up. The antenna system at the measurement site routes the received energy

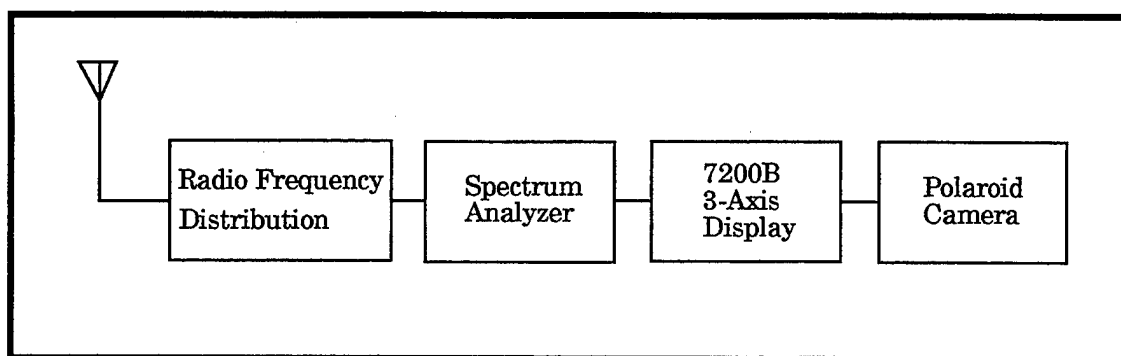


Figure A.1: Field Data Measurement Setup

through a radio frequency distribution system to an output port. The RF output is then connected, generally through a band-pass filter, to a HP-141 series scanning spectrum analyzer. An ELF Engineering Model 7200B 3-Axis Display (hereafter referred to as a 3-axis display), is utilized in conjunction with the scanning spectrum analyzer to view the temporal and spectral properties of the received energy.

1. Radio Frequency Distribution

At each field site, except for the NPS site, the antenna feed was routed through a RF distribution system to various ancillary equipment. Prior to data measurements taken for this investigation, the host receiving system was analyzed for gain/loss parameters from antenna to the RF output port

feeding the spectrum analyzer. If any RF path was not within the system specifications it was not utilized for data measurement.

At the NPS site the receive signal was not routed through a distribution system; the antenna was connected, through a band-pass filter, directly to the spectrum analyzer.

2. Hewlett-Packard Spectrum Analyzer

A Hewlett-Packard, Model HP-141T, was the spectrum analyzer utilized as the scanning receiver. This analyzer has interchangeable RF modules to cover various frequency ranges. The majority of the measurements for this thesis were taken using the 8553B model RF module which covers the 10 kHz to 11 MHz and 10 kHz to 110 MHz frequency range; otherwise the 8554B model RF module (10 kHz to 1200MHz) was used. A key feature of these modules is the variety of input-bandwidth, scan-width, and attenuation settings. The HP-141T also has an Intermediate Frequency (IF) section that controls scan-time and provides scan synchronization with the power-line frequency.

The HP-141T has rotating knob-type controls that allow the operator to quickly change various analyzer settings. Rapid manual intervention by the equipment operator is usually required to capture specific or unique SOI temporal and spectral characteristics of man-made noise and SOI. Unfortunately, many newer model spectrum analyzers have a digital keypad type input which does not allow the rapid changing of the measurement parameters required to isolate and define the specific temporal and spectral characteristics of power-line noise.

The HP-141T can synchronize the beginning of a scan sequence with the fundamental frequency of the power being applied to the equipment. This mode of operation is referred to as "line sync." The ability to switch the spectrum analyzer between the line sync and non-line sync mode of operation

is paramount to power-line-noise identification. Power-line noise will show up as diagonal lines on the 3-axis display when the analyzer (not line synchronized) is set to scan a wide band of the frequency spectrum, and the time per spectral band scan is longer than the repetitive period of the line power (16.6 ms for 60-Hz operation and 20 ms for 50-Hz operation). Figure A.2 is an example of power-line noise when viewed on the 3-axis display while the analyzer is not in the power-line sync mode of operation. When the spectrum analyzer is switched to the line-sync mode of operation the power-line-noise impulses become synchronized with the scanning receiver and consequently will align parallel to the time axis of the 3-axis display. Figure A.3 shows an example of power-line noise when viewed on the 3-axis display while in the line-sync mode of operation.

a. Radio Frequency Spectrum Filters

The HF radio band contains numerous strong signals in addition to low-level SOI's. An analyzer requires a considerable dynamic range of operation to examine low-level signals that reside in this type of spectral environment. The spectral range requirements for which data in this investigation was collected exceeded the dynamic range of the HP-141T. Consequently, filters were utilized to reduce the total signal- and noise-power delivered to the spectrum analyzer.

The dynamic range of ambient signals can also exceed the dynamic range of the pre-amplifiers. If this occurs intermodulation products can be generated. Intermodulation products corrupt the measured data. Consequently, a bank of filters was employed to reduce the total signal and noise power fed to the instrumentation. The filter banks are custom designed for use for in specific parts of the world. Table A.1 lists a typical bank of filters and the corresponding frequency range. The majority of the filters were designed to pass narrow spectral bands located between allocated

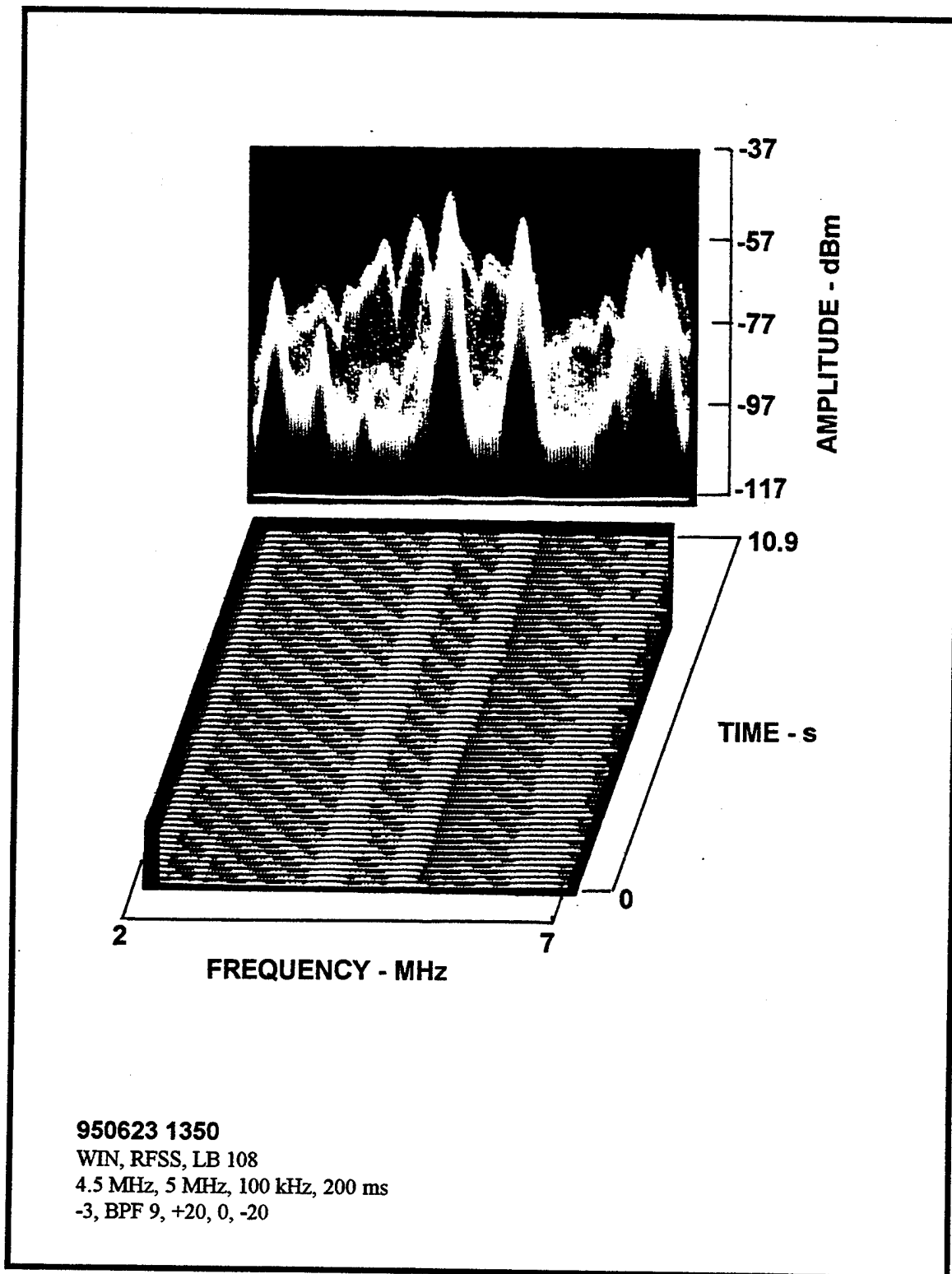
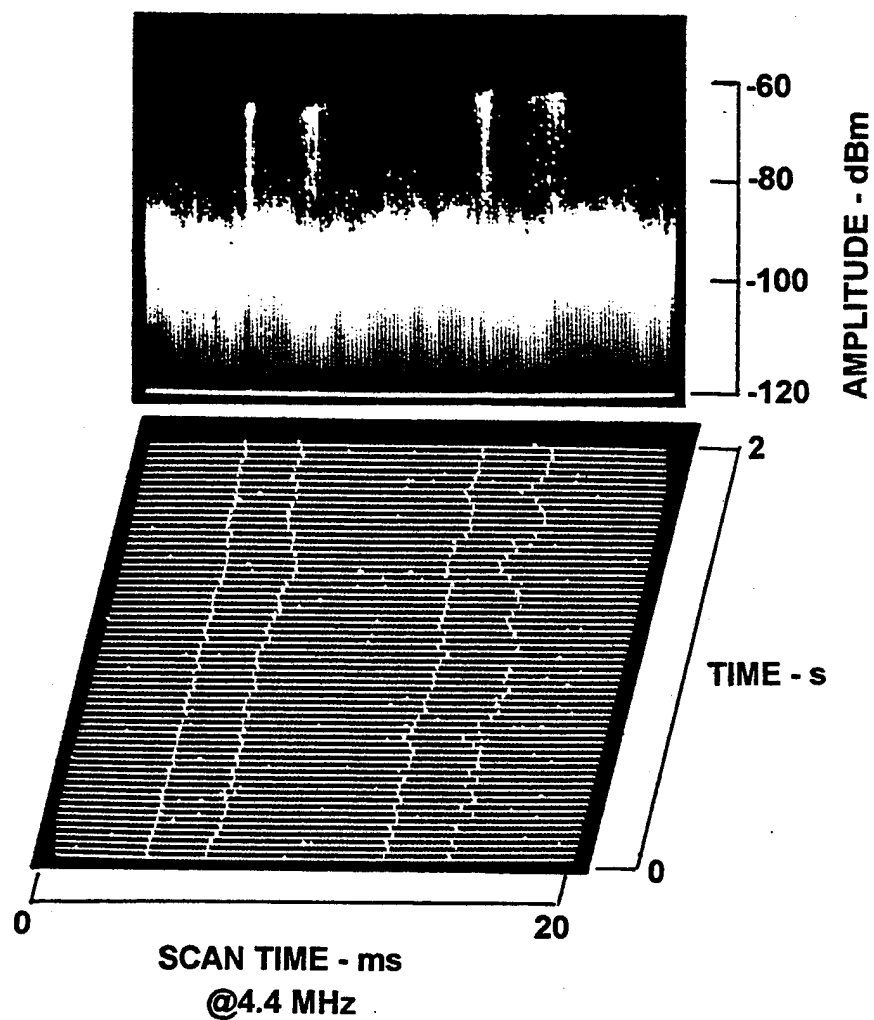


Figure A.2: Power-line Noise Viewed on a 3-axis Display While the Spectrum Analyzer is not Line Synchronized.



950622 1200
WIN, RFSS, CM
4.4 MHz, 0, 30 kHz, 20 ms LS
BPF 1, +20, 0, -20

Figure A.3: Power-line Noise Viewed on a 3-axis Display While the Spectrum Analyzer is Line Synchronized.

international broadcast service bands. The broadcast bands contain very strong signals that would easily overwhelm the dynamic range of the analyzer, particularly if viewing wide portions of the HF radio spectrum.

Table A.1: Typical Bank of Filters

Filter	Frequency Range (MHz)
1	1.95 – 5.90
2	6.15 – 9.45
3	9.85 – 11.60
4	12.00 – 13.60
5	13.75 – 15.05
6	15.55 – 17.50
7	17.85 – 21.40
8	21.85 – 25.65
9	2.0 – 8.0
10	2.0 – 30.0

3. ELF Engineering Model 7200B 3-axis Display

The ELF Engineering 7200B 3-axis display provides a time history of the spectrum analyzer scans. As the analyzer scans a frequency range (or time scans a single frequency) the output is ported to the 3-axis display. The data from each scan is stored (a maximum of 60 independent scans), in an internal digital memory. The 3-axis front panel display represents data as a moving real-time quasi-continuous process. Figure A.4 is an overall diagram of the visual representation process. The front panel output motion is coupled to the scanning time of the analyzer; hence, the display can move slowly or quickly depending on the needs of the operator. The resulting three dimensional block of data can be manipulated by controlling the elevation,

rotation, and compression of the axes to view the time history in any convenient way. The motion of the display can also be stopped at any time for viewing. While the display is stopped Polaroid photographs are taken to provide a hard copy data record.

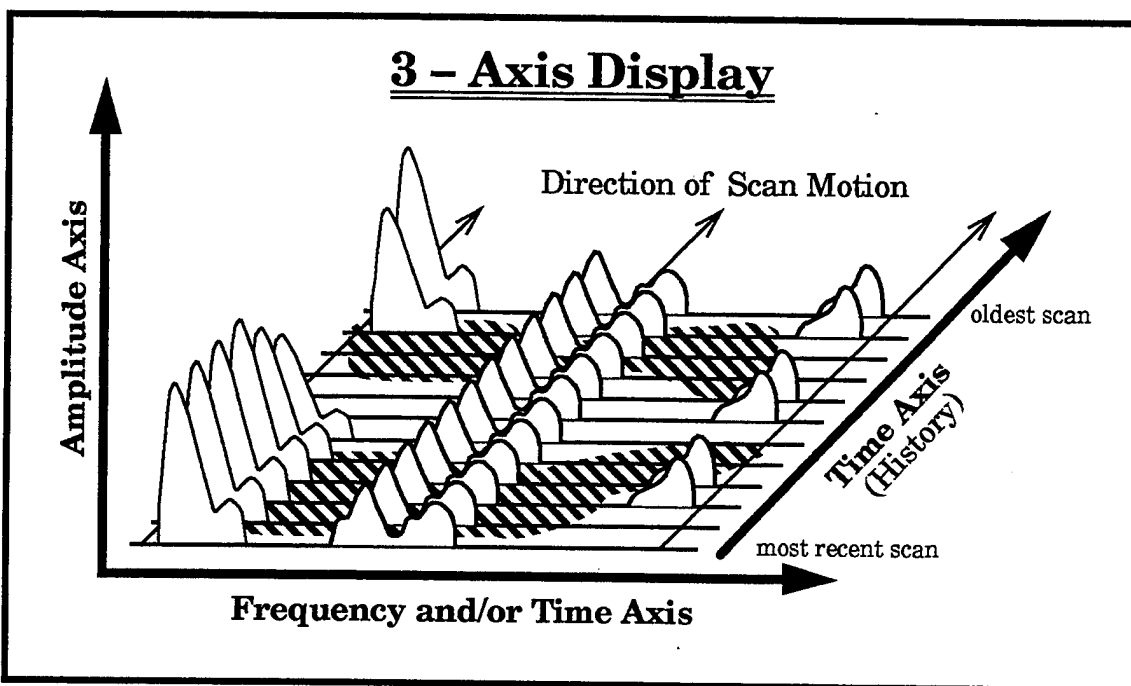


Figure A.4: Scanning Diagram for the 3-Axis Display

4. Tektronix C5-C Camera

A Tektronix C5-C Polaroid camera was utilized to take still photographs of the 3-axis display. The Polaroid photograph provides a convenient record of the temporal and spectral conditions witnessed during data collection.

Prior to data measurements the spectrum analyzer is calibrated. Various calibrated levels of the analyzer are ported to the 3-axis display, stored, and photographed. The photographic record is used to generate an accurate measurement scale that one can use to extrapolate the amplitude value of all further photographic data.

B. INFORMATION IDENTIFICATION MATRIX

Each figure formatted from a Polaroid photograph contains an information matrix. The entries provide all the necessary information concerning the parameters of the data.

Time	Date		
Site	Specific Measurement Location		
Center Frequency	Scan Width	IF Bandwidth	Scan Time
Filter #	Preamplifier (dB)	Input Attenuation	IF Gain

Figure A.5: Polaroid Photograph Information Matrix

APPENDIX B. DATA COLLECTION LOCATIONS

This appendix describes the field measurement locations.

A. HAN

- Location: Okinawa, Japan
- Antenna: CDAA
- CCIR class: Rural/Residential
- Description: The site is not on a hill top, however, it does have an elevated view of the surrounding area. To the North East, West, and South West are small towns.

B. LAH

- Location: Los Altos Hills, California
- Antenna: Log Periodic mounted on 50 ft mast
- CCIR class: Residential
- Description: Sparsely populated. Area contains rolling hills shadowed from the North by gradual rise in hill elevation. Area contains overhead power-lines.

C. MSA DET J

- Location: Asian area country
- Antenna: Log Periodic mounted on 20 ft mast
- CCIR class: Rural
- Description: Located on a hill top. There are no nearby residences or towns within 30-km line-of-site. An adjacent hill top 2-km away has

a small building. Commercial power is provided to MSA Det J and to the building by an overhead distribution line.

D. MSA DET L

- Location: Asian area country
- Antenna: Log Periodic mounted on 20 ft mast
- CCIR class: Rural
- Description: It is located on a hill top. To the East is located a small town and sparsely scattered about the East and South East are residences.

E. NPS

- Location: Monterey, California
- Antenna: Log Periodic mounted on a 85 ft tower
- CCIR class: Residential
- Description: It is located on a hill side that has gently sloping terrain coming up from the ocean. There are many hills surrounding this location (approximately 10-km distance) that are higher than this location. The site is located in the middle of a housing area that contains overhead power-lines.

F. WIN

- Location: Winter Harbor, Maine
- Antenna: CDAA
- CCIR class: Rural
- Description: It is located on the coast and is primarily surrounded by water. To the South West is located a small town and the

surrounding area is sparsely populated. Commercial power to this site is supplied via underground power-lines that enter a cable head from overhead power-lines approximately 1-km away.

LIST OF REFERENCES

1. International Radio Consultative Committee (CCIR), CCIR Report 258-5, "Man-Made Radio Noise," Geneva, Switzerland, 1990.
2. Hagn, G. H., "Definitions and Fundamentals of Electromagnetic Noise, Interference, and Compatibility," *AGARD Conference Proceedings Na 159 on Electromagnetic Noise Interference and Compatibility*, pp. 1.1 - 1.24, November 1975.
3. International Radio Consultative Committee (CCIR), CCIR Report 322-3, "Characteristics and Applications of Atmospheric Radio Noise Data," Geneva, Switzerland, 1988.
4. Goodman, J. M., *HF Communication, Science & Technology*, Van Nostrand Reinhold, New York, New York, 1992.
5. Meek, J. M., and Craggs, J. D., (Editors), *Electrical Breakdown of Gases*, John Wiley & Sons, New York, New York, 1978.
6. Beasley, W. L., "An Investigation of the Radiated Signals Produced by Small Sparks on Power Lines," Ph.D. Dissertation, Texas A&M University, College Station, Texas, January 1980.
7. O'Dwyer, J. M., "Electromagnetic Noise and Interference at High Frequency Communications Receiver Facilities," Master's Thesis, Naval Postgraduate School, Monterey, California, June 1984.
8. O'Dwyer, J. M., "Power Line Noise Models and Energy Detection in the High Frequency Radio Band," Ph. D. Dissertation, Naval Postgraduate School, Monterey, California, June 1986.
9. Parkala, W. E., Taylor, E. R., and Harrold, R. T., "Radio Noise Measurements on Overhead Power Lines from 2.4 to 345 kV," *IEEE International Symposium on Electromagnetic Compatibility*, IEEE 68C12-EMC, pp. 96-107, 1968.
10. Parkala, W. E., and Chartier, V. L., "Radio Noise Measurements on Overhead Power Lines from 2.4 to 800 kV," *IEEE Trans. on Power Apparatus and Systems*, vol. PAS-90, no. 3, pp. 1155-1165, May/June 1971.

11. Skomal, E. N., *Man-Made Radio Noise*, Van Nostrand Reinhold, New York, New York, 1978.
12. Vincent, W. R., and Munsch, G. F., *Signal-to-Noise Enhancement Program Power-Line Noise Mitigation Handbook*, 2d edition, prepared for Headquarters, Naval Security Group, Washington, D. C., January 1993.
13. Vincent, W. R., Private communication with the author, November, 1995.
14. Warburton, F. W., Liao, T., and Hoglund, N. A., "Power Line Radiations and Interference Above 15 MHz," *IEEE Trans. on Power Apparatus and Systems*, vol. PAS-88, no. 10, pp. 1492-1501, October 1969.
15. IEEE Transmission and Distribution Committee, "Review of Technical Considerations on Limits to Interference from Power Lines and Stations," *IEEE Trans. on Power Apparatus and Systems*, vol. PAS-99, no. 1, pp. 365-388, January/February 1980.
16. IEEE Transmission and Distribution Committee, "A Field Comparison of RI and TVI Instrumentation," *IEEE Trans. on Power Apparatus and Systems*, vol. PAS-96, no. 3, pp. 863-875, May/June 1977.
17. Limberger, E. N., "Locating Radio Frequency Interference on Power Transmission Lines," *IEEE Conference Paper*, IEEE paper no. 92C3, 1992.
18. Spaulding, A. D., and Washburn, J. S., "Atmospheric Radio Noise: Worldwide Levels and Other Characteristics," NTIA Report 85-173, National Telecommunications and Information Administration, U.S. Department of Commerce, 1985.
19. Spaulding, A. D., and Disney, R. T., "Man-Made Radio Noise, Part I: Estimates for Business, Residential, and Rural Areas," OT Report 74-38, Office of Telecommunications, U.S. Department of Commerce, June 1974.
20. Spaulding, A. D., and Stewart, F. G., "An Updated Noise Model for Use in IONCAP," NTIA Report 87-212, National Telecommunications and Information Administration, U.S. Department of Commerce, January 1987.
21. International Radio Consultative Committee (CCIR), CCIR Report 670-1, "Worldwide Minimum External Noise Levels, 0.1 Hz to 100 GHz," Geneva, Switzerland, 1990.

22. IEEE Joint Technical Advisory Committee, "Spectrum Engineering—The Key to Progress," IEEE, Inc., New York, New York, 1968.
23. Lauber, W. R., "Radio Noise Surveys at Canadian HF Communication Sites," *IEEE Trans. on Electromagnetic Compatibility*, vol. EMC-19, no. 2, pp. 44-49, May 1977.

BIBLIOGRAPHY

Allen, E. W., *The Radio Noise Spectrum*, (D. H. Menzel, Ed.), Harvard University Press, Cambridge, Massachusetts, 1960.

Apostolakis, D., Katsikis, M., and Constantinou, P., "Man Made Noise Measurements," IEEE order no. CH2964-5/91/0000-0641, pp. 641-642, 1991.

Arafiles, V. P. and Valdez, I., "Power Line Noise Effects and New Radio Noise Models," *IEEE International Symposium on Electromagnetic Compatibility, Symposium Record*, pp. 51-52, 9-13 August 1993.

Audone, B., and Franzini-Tibaldeo, G., "Broad-Band and Narrow-Band Measurements," *IEEE Trans. on Electromagnetic Compatibility*, vol. EMC-15, no. 2, pp. 66-71, May 1973.

Berry, L. A., "Understanding Middleton's Canonical Formula for Class A Noise," *IEEE Trans. on Electromagnetic Compatibility*, vol. EMC-23, no. 4, pp. 337-344, November 1981.

Beuhler, W. E., and Lunden, C. D., "Signature of Man-Made High-Frequency Radio Noise," *IEEE Trans. on Electromagnetic Compatibility*, vol. EMC-8, no. 3, pp. 143-152, September 1966.

Bolton, E. C., "Man-Made Noise Study at 76 and 200 kHz," *IEEE Trans. on Electromagnetic Compatibility*, vol. EMC-18, no. 3, pp. 93-96, August 1976.

Bridges, E., Goddard, W. R., Gad, T., and Boerner, W-M., "Measurement and Study of Radio Noise from Electric Power Lines in the Central Canada Region," *1980 IEEE International Symposium on Electromagnetic Compatibility Record*, pp. 21-25, Baltimore, Maryland, October 1980.

Fraser-Smith, A. C., and Bowen, M. M., "The Natural Background Levels of 50/60 Hz Radio Noise," *IEEE Trans. on Electromagnetic Compatibility*, vol. EMC-34, no. 3, pp. 330-337, August 1992.

German, J. P., "Characteristics of Electromagnetic Radiation from Gap-Type Spark Discharges on Electric Power Distribution Lines," *IEEE Trans. on Electromagnetic Compatibility*, vol. EMC-11, no. 2, pp. 83-89, May 1969.

Giordano, A. A., "Electromagnetic Noise and Interference (Chapter 5)," *Review of Radio Science, 1981-1983*, Bowhill, S. A., Editor, International Union of Radio Science, (URSI), Brussels, Belgium, 1984.

Gupta, M. S., (Editor), *Electrical Noise: Fundamentals & Sources*, IEEE Press, New York, New York, 1977.

Hagn, G. H., "Radio Noise of Terrestrial Origin (Chapter 8)," *Review of Radio Science, 1972-1974*, Bowhill, S. A., Editor, International Union of Radio Science, (URSI), Brussels, Belgium, 1975.

Hagn, G. H., and Shephard, R. A., "Man-made Electromagnetic Noise from Unintentional Radiators: A Summary," *AGARD Conference Proceedings No 159 on Electromagnetic Noise Interference and Compatibility*, pp. 3.1-3.24, November 1975.

Hagn, G. H., "Interference Environment (Chapter 6)," *Review of Radio Science, 1975-1977*, Bowhill, S. A., Editor, International Union of Radio Science, (URSI), Brussels, Belgium, 1978.

Hagn, G. H., "Definitions of Electromagnetic Noise and Interference," *1977 IEEE International Symposium on Electromagnetic Compatibility*, pp. 122-127, 2-4 August 1977.

Herman, J. R., "Survey of Man Made Radio Noise," *Progress in Radio Science 1966-1969*, vol. 1, pp. 315-347, URSI, 1970.

IEEE Radio Noise Subcommittee Report, "Comparison of Radio Noise Prediction Methods with CIGRE/IEEE Survey Results," *IEEE Trans. on Power Apparatus and Systems*, vol. PAS-92, no. 3, pp. 1029-1042, May/June 1973.

IEEE Transmission and Distribution Committee, "Transmission System Radio Influence," *IEEE Trans. on Power Apparatus and Systems*, vol. PAS-84, no. 8, pp. 714-724, August 1965.

Jauregui, S., Adler, R., and Vincent, W. R., *SNEP Study Manual*, Technical Manual, Draft 1, April 1991.

Lott, G. K., Vincent, W. R., and Jauregui, S., "HF Signal Amplitude Distributions and Total Spectrum Power Measurements," *HF Radio Systems and Techniques*, IEE Conference Publication No. 392, pp. 140-143, July 1994.

Malik, N. H., and Al-Arainy, A. A., "EMI Characteristics of Distribution Lines Located in Desert Lands," *IEEE Trans. on Electromagnetic Compatibility*, vol. EMC-31, no. 3, pp. 273-279, August 1989.

March, D., "EMC Measurements Before and After Construction of a 500 KV Line Show Surprising Results," *1981 IEEE International Symposium on Electromagnetic Compatibility Record*, pp. 531-535, Boulder, Colorado, August 1981.

Matheson, R. J., "Instrumentation Problems Encountered Making Man-Made Electromagnetic Noise Measurements for Predicting Communication System Performance," *IEEE Trans. on Electromagnetic Compatibility*, vol. EMC-12, no. 4, pp. 151-158, November 1970.

Menzel, D. H., (Editor), *The Radio Noise Spectrum*, Harvard University Press, Cambridge, Massachusetts, 1960.

Middleton, D., "Statistical-Physical Models of Urban Radio-Noise Environments—Part I: Foundations," *IEEE Trans. on Electromagnetic Compatibility*, vol. EMC-14, no. 2, pp. 38-56, May 1972.

Middleton, D., "Statistical-Physical Models of Electromagnetic Interference," *IEEE Trans. on Electromagnetic Compatibility*, vol. EMC-19, no. 3, pp. 106-127, August 1977.

Owen, R. E., Vincent, W. R., and Blair, W. E., "Measurement of Impulsive Noise on Electric Distribution Systems," *IEEE Trans. on Power Apparatus and Systems*, vol. PAS-99, no. 6, pp. 2433-2438, November/December 1980.

Roy, T. N., "Airborne Man-Made Radio Noise Assessment," *1982 IEEE International Symposium on Electromagnetic Compatibility Record*, pp. 288-295, September 1982.

Saha, J. N., "The Radio Interference Field of an Overhead Transmission Line," *IEEE Trans. on Electromagnetic Compatibility*, pp. 38-40, November 1971.

Sailors, D. B., "A Discrepancy in the International Radio Consultative Committee Report 322-3 Radio Noise Model: The Probable Cause," *Radio Science*, vol. 30, no. 3, pp. 713-728, May-June 1995.

Sheikh, A. U. H., and Parsons, J. D., "Statistics of Electromagnetic Noise Due to High-Voltage Power Lines," *IEEE Trans. on Electromagnetic Compatibility*, vol. EMC-23, no. 4, pp. 412-419, November 1981.

Skomal, E. N., "An Analysis of Metropolitan Incidental Radio Noise Data," *IEEE Trans. on Electromagnetic Compatibility*, vol. EMC-15, no. 2, pp. 45-57, May 1973.

Skomal, E. N., and Smith Jr., A. A., *Measuring the Radio Frequency Environment*, Van Nostrand Reinhold Company, New York, 1985.

Smith Jr., A. A., "Power Line Noise Survey," *IEEE Trans. on Electromagnetic Compatibility*, pp. 31-32, February 1972.

Spaulding, A. D., Ahlbeck, W. H., and Espeland, L. R., "Urban Residential Man-Made Radio Noise Analysis & Predictions," OT/TRER 14, Telecommunications Research and Engineering Report 14, Office of Telecommunications, U.S. Department of Commerce, June 1971.

Spaulding, A. D., and Disney, R. T., "Man-Made Radio Noise, Part II: Bibliography of Measurement Data, Applications, and Measurement Methods," OT Report 75-63, Office of Telecommunications, U.S. Department of Commerce, May 1975.

Spaulding, A. D., and Hagn, G. H., "Worldwide Minimum Environmental Radio Noise Levels (0.1 Hz to 100 GHz)," *Proceedings 1978 Symposium on the Effect of the Ionosphere on Space and Terrestrial Systems*, pp. 1-6, January 1978.

Stuart, G. F., and Sites, M. J., "Man-Made Radio Noise Levels at 150 kHz to 32 MHz Near a Large Antarctic Base," *IEEE Trans. on Electromagnetic Compatibility*, vol. EMC-15, no. 3, pp. 93-99, August 1973.

Stumpers, F. L. H. M., "Progress in the Work of CISPR," *IEEE Trans. on Electromagnetic Compatibility*, vol. EMC-12, no. 2, pp. 29-32, May 1970.

Thomas Sr., L. W., "EMC Twenty Years Ago," *IEEE Trans. on Electromagnetic Compatibility*, vol. EMC-20, no. 4, pp. 473-482, November 1978.

Vincent, W. R., "Examples of Signals and Noise in the Radio-Frequency Spectrum," *IEEE Trans. on Electromagnetic Compatibility*, vol. EMC-19, no. 3, pp. 241-253, August 1977.

Vincent, W. R., Smith, D., and Jauregui, S., "Temporal and Spectral Properties of Power-Line Noise," *1980 IEEE International Symposium on Electromagnetic Compatibility Record*, pp. 26-29, Baltimore, Maryland, October 1980.

Vincent, W. R., "Practical Aspects of Man-Made Radio Noise that Affect Radio-Spectrum Management," *1980 IEEE International Symposium on Electromagnetic Compatibility Record*, pp. 107-109, Baltimore, Maryland, October 1980.

Vincent, W. R., "Radio Noise and Interference (Chapter 34)," *Reference Data for Engineers: Radio, Electronics, Computer, and Communications*, Seventh Edition, Howard W. Sams & Co., Indianapolis, Indiana, 1989.

Volland, H., (Editor) *CRC Handbook of Atmospherics, Volume 1*, CRC Press, Inc., Boca Raton, Florida, 1982.

INITIAL DISTRIBUTION LIST

1. Defense Technical Information Center 2
8725 John J. Kingman Rd., STE 0944
Ft. Belvoir, VA. 22060-6218

2. Dudley Knox Library, Code 013..... 2
Naval Postgraduate School
Monterey, CA. 93943-5101

3. Director, Training and Education 1
MCCDC, Code C46
1019 Elliot Rd.
Quantico, VA 22134-5027

4. Chairman, Code EC..... 1
Department of Electrical and Computer Engineering
Naval Postgraduate School
Monterey, CA. 93943-5121

5. Prof. Richard W. Adler, Code EC/Ab..... 3
Department of Electrical and Computer Engineering
Naval Postgraduate School
Monterey, CA. 93943-5121

6. Prof. Wilbur R. Vincent, Code EC/Ab 5
Department of Electrical and Computer Engineering
Naval Postgraduate School
Monterey, CA 93943-5121

7. Commander Gus Lott, USN, Code EC/Lt..... 1
Department of Electrical and Computer Engineering
Naval Postgraduate School
Monterey, CA 93943-5121

8. Prof. Rasler W. Smith, Code EC/Sr 1
Department of Electrical and Computer Engineering
Naval Postgraduate School
Monterey, CA 93943-5121

9. Commander Naval Security Group, N44 1
Attn: Ms. Jackie Sherry
9800 Savage Rd.
Ft. George G. Meade, MD 20755-6000
10. Commander John M. O'Dwyer, USN..... 1
Naval Information Warfare Activity, Code N9
9800 Savage Rd.
Ft. George G. Meade, MD 20755-6000
11. Commander United States Army Intelligence and Security Command 1
IAMSА-V-EAQ (Attn: Ms. Anne Biligihan)
Vint Hill Farms, Bldg. 160, MS 26
Warrenton, VA 22186-5160
12. Commander Naval Command and Control and Ocean Surveillance 1
Center In-Service Engineering EAST
Attn: Mr. Steve Kelly, Code 722SK
4600 Marriott Drive
North Charleston, SC 29406
13. Commander Naval Command and Control and Ocean Surveillance 1
Center In-Service Engineering WEST
Attn: Mr. Brian Kutara
675 Lehua Avenue
Pearl City, HI 96782-3356
14. Mr. James Breakall 1
The Pennsylvania State University Applied Research Laboratory
P. O. Box 30
State College, PA 16804
15. Mr. Alan G. Sonsteby 1
The Pennsylvania State University Applied Research Laboratory
P. O. Box 30
State College, PA 16804
16. Mr. Mark Beighey..... 1
ManTech Field Engineers
HSC 751st Military Intelligence Battalion
Unit Number 15276, Box 721
APO AP96271-0162

17. Dr. William Blair. 1
Electric Power Research Institute
3412 Hillview Avenue
Palo Alto, CA 94025
18. Mr. George Hagn. 1
Stanford Research Institute, International
1611 North Kent St.
Arlington, VA 22209
19. Mr. Wally Hanifin. 1
Pacific Gas and Electric
De Anza Division
10860 North Blaney Avenue
Cupertino, CA 95014
20. Mr. Carlos Milnick. 1
Engineering Research Associates
1595 Springhill Rd.
Vienna, VA 22180
21. Mr. George Munsch. 1
160 CR 375
San Antonio, TX 78253
22. Captain James W. Hodge Jr., USMC. 2
P.O. Box 133
Quantico, VA 22134